The Dissertation Committee for Young-Hoon Han certifies that this is the approved version of the following dissertation:

Fatigue Life Prediction for Cord-Rubber Composite Tires Using a Global-Local Finite Element Method

Committee:

Eric P. Fahrenthold, Supervisor

Eric B. Becker, Co-Supervisor

H. Grady Rylander

Alfred E. Traver

Raul G. Longoria

Sebnem Özüpek

Fatigue Life Prediction for Cord-Rubber Composite Tires Using a Global-Local Finite Element Method

by

Young-Hoon Han, BS, MS

Dissertation

Presented to the Faculty of the Graduate School of

The University of Texas at Austin

in Partial Fulfillment

of the Requirements

for the Degree of

Doctor of Philosophy

The University of Texas at Austin

May, 2003

“For no matter how many promises God has made,
they are ‘Yes’ in Christ.
And so through him the ‘Amen’ is spoken
by us to the glory of God.”
(2 Corinthians 1:20)

“Give thanks in all circumstances,
for this is God’s will for you in Christ Jesus.”
(1 Thessalonians 5:18)

To my Lord,
and
To my Family

Acknowledgements

Thank you Dr. Eric P. Fahrenthold, supervisor, and Dr. Eric B. Becker, co-supervisor for the motivation, encouragement and invaluable suggestions during the course of this investigation.

Thank you also to the members of my committee, Drs. H. Grady Rylander, Alfred E. Traver, Raul G. Longoria and Sebnem Özüpek for serving on the supervising committee.

To my former employer, Hankook Tire Company, thanks for initial financial support, and also to the Texas Advanced Computing Center at the University of Texas at Austin for providing computer time support.

Most importantly, to my wife, Ki-Soon and children, Jung-Hyun, Hyun-Soo and Hyun-Jae, thank you for the sacrifice and encouragement as I worked to complete this dissertation. Thank you also to father, though he was passed away last year, and to mother, brothers and sisters for all the year of their encouragement.

This work was supported in part by the National Science Foundation (CMS99-12475) and the Bandag Ltd.

Fatigue Life Prediction for Cord-Rubber Composite Tires Using a Global-Local Finite Element Method

Publication No._____

Young-Hoon Han, PhD.

The University of Texas at Austin, 2003

Supervisors: Eric P. Fahrenthold and Eric B. Becker

A failure analysis, based on fracture mechanics, may be useful for predicting the lifetime of a cord-reinforced rubber composite pneumatic tire. This study presents a new 3D FE local model to calculate the energy release rate at the vulnerable region, belt edge. The new local model uses a three-dimensional FEM fracture analysis, based on a steady-state rolling assumption, in conjunction with a global-local technique in ABAQUS. Within the local model, J-integral variation study is performed in the crack region. Furthermore, it is used to determine the crack growth rate analysis. This study assumes that a flaw exists inside the tire, in the local model, due to a mechanical inhomogeneity introduced in the manufacturing of the tire. This paper also considers how different driving conditions, such as

free-rolling, braking, traction, and lateral load contribute to the detrimental effects of belt separation in tire failure.

Table of Contents

CHAPTER I

INTRODUCTION

1.1 General

The structure of a pneumatic tire consists of layers of reinforced cords. These cords are made up of an assortment of several different useful fibers, synthetics, or metals. These cords are in turn imbedded in a matrix whose composition is formed by either natural rubber compounds, compounds of numerous synthetic elastomers, or composites of both. Composites have widely been selected for the construction of pneumatic tires because of their multifunctional properties; for example the aeronautical and automotive industries find composites to be very useful because they are able to provide a high degree of stiffness in both the lateral and longitudinal directions. As a result of their widespread use, it has become increasingly important to accurately evaluate the properties of composites as they relate to the design variables[1] of pneumatic tires. A major issue concerning one particular variable—tire belts, has led the inability to accurately predict the lifetime or durability of a pneumatic tire. This variable demands attention, as tire failure due to belt separation during tire operation at tire lifetime limits can be sudden causing dangerous vehicle instability.

[1] belt angle, belt width, interlaminar rubber gage, etc.

Focused research in tire mechanics has been performed to enhance tire (belt) durability during the last decade. The research concentrates on two main approaches to determine the durability of a pneumatic tire (belt) through computer aided engineering: (1) design variable analysis using a continuum finite element model; and (2) fracture mechanics analysis using a finite element method. The design variable analysis using a continuum finite element model approach has concentrated its research efforts on the parametric analysis of the pneumatic tire's design variables. Typically, this approach compares design variable values such as strain energy, von Mises stress, maximum normal stress, maximum shearing strain, hydrostatic stress, and belt edge shear strain to the values for different material of structural configurations. Specifically this approach has played a key role in developing more durable tires from quantitative comparison of durability in a finite element model. The fracture mechanics analysis using a finite element method has concentrated its efforts on the failure analysis of cord-reinforced rubber composites in tires. This approach has emerged as an important tool for the quantitative comparison of finite element results to predict the lifetime of a pneumatic tire. This approach bases its analysis on the assumption that there is a pre-existing flaw inside the tire due to a mechanical in-homogeneity produced in the manufacturing process. By virtue of this assumption the tire belt durability

may be characterized by the initiation of failure at the belt edge region induced by belt separation of the composite.

However, all previous research implementing fracture mechanics analysis using a finite element method has used simplified two-dimensional or three-dimensional models that consist of only one-directional flaws due to the difficulty arising from the conversion, in the numerical sense, mechanical load to energy release rate. This dissertation presents a study of tire durability using a three-dimensional cylindrical shape of a local crack model for the calculation of the energy release rate, to assist in predicting the lifetime of a pneumatic tire. The principal advantages of this local model are: (1) there are no singularity problems in the J-integral calculation; (2) the direction of crack propagation can be predicted by J-integral values, along the crack fronts; and (3), the cost efficiency associated with the use of a global-local technique is advantageous.

1.2 Literature Review

Fracture mechanics for structural evaluation has been used to consider an existing initial flaw inside the structure since Griffith's introduction of the concept of the energy release rate. Most previous works for the tire fracture mechanics relied on the experimental measurements of rubber components since

the methods for predicting tire belt separation are currently becoming feasible in analytic and computational techniques.

A testing of rubber specimen [1,3,6,13] is the simplest way for finding fatigue phenomena in complicated tire structure behavior, with respect to various loading conditions and specimen types. A. Stevenson [1] used a rubber discs bonded to metal endpieces for an experiment the energy release rate. The energy release rate was obtained by virtue of the load-deflection curve, at several intermediate stages of crack growth. This is the conventional technique to get the energy release rate from load-deflection curve by Instron machine. An analytical form of energy release rate of a cylinder rubber block in compression was suggested in terms of shear modulus G, dimensional parameters r, d, k, and surface strain e_s:

$$T = \frac{6G(r-k)(1+2S^2)e_s^{\,2}}{\frac{3d}{2(r-k)}\sinh^{-1}\frac{2(r-k)}{d} + \frac{6(r-k)}{d}\sqrt{1+\frac{d^2}{4(r-k)^2}}}. \qquad (1.1)$$

He also validated the relationship between conventional fatigue crack growth test results and analytical results, and found good correspondence. D. G. Young [3] and G. P. Giuliani [13] introduced pure shear test and mixed mode loading test,

respectively. Very recently, Giuliani [13] suggested tearing energy equation using shear test results for belt edge by incompressible material condition:

$$T = \frac{1}{2} G \gamma_{xy}^2 h, \tag{1.2}$$

in which, G is the shear modulus and h is the rubber layer thickness.

On the other hand, a finite element approach [4,5,7,10,11] is an alternative method to find out the energy release rate (J-integral), and predict a lifetime. Becker [4] extended the virtual crack extension method to the domain integral method for calculating energy release rate in which non-conservative crack surface tractions are considered, and gave a method for evaluating it from finite element results. Pidaparti [5] calculated energy release rate using virtual crack extension method of a two-dimensional plane stress finite element model, and he considered the cord angle change due to a large extension. In 1996, T. G. Ebbott [7] first utilized two-dimensional plane strain tire model for predicting the number of cycles in a real tire, specially focused in the bead separation. He modeled an initial flaw near the bead turn-up area with the assumption of crack existence, ribbon type, around the circumference. After Ebbott's works on finite element analysis, based on fracture mechanics, three-dimensional fracture analysis [10,11] for a tire were performed in recent years. The weak point of these past studies was only one-direction crack was considered in the three-dimensional model. It made a difficulty in showing the variation of energy release rate in both directions

therefore; there were difficulty in predicting real lifetime of a tire. These literature surveys motivated a current research for more reasonable and tangible method to predict a tire lifetime.

Related works with an energy release rate for composite materials are introduced here. Many people have considered interface delamination problems [15-17,19,21,27]. An elastic damage model, equation (1.3), for mixed-mode delamination in fiber composites is illustrated [21,22], and used to simulate plane strain finite element model containing interface elements.

$$\bar{\sigma} = \begin{Bmatrix} \bar{\sigma}_I \\ \bar{\sigma}_{II} \end{Bmatrix} = [\, I - D \,] E_0 \begin{Bmatrix} \bar{\varepsilon}_I \\ \bar{\varepsilon}_{II} \end{Bmatrix} = \left[I - \frac{k}{1+k} F \right] E_0 \bar{\varepsilon} \,. \qquad (1.3)$$

In equation (1.3) E_0 is a diagonal matrix containing the initial stiffness in mode I and II, and F is another diagonal matrix. The main feature of this damage model is that no initial flaws are required. He also suggested the simple closed form of energy release rate, as applied to a bending specimen.

$$G = \frac{3P^2 a^2}{16 b^2 h^3 L^2 E_{11}} [\, 4(3c - L)^2 + 3(c + L)^2 \,] \,. \qquad (1.4)$$

The dimensional parameters of equation (1.4) are represented in Figure 1.1. Mars, W. V. [28] utilized the damage technique for obtaining cracking energy density from the total elastic strain energy density. He expressed cracking energy density as in terms of the crack orientation, the transformation between the principal and

original coordinates. D. Dalmas and A. Laksimi represented [30] strain energy release rate using R ratio, $R = P_{\min} / P_{\max}$, to differentiate mode I and mode II.

$$\Delta G = kG_{max}, \tag{1.5}$$

with $k = (1 - R^2)$, $k = (1 - R)^2$ for mode I and mode II respectively. Another interesting study in composite interlaminar fracture is focusing on the three-dimensional stress state in the interplay ahead of the crack tip [31]. This study claimed that the dominant stresses associated with individual fracture modes are easily recognized from three-dimensional finite element analysis, and comparison of stress magnitudes ahead of the crack tip with corresponding local laminate strengths leads to the dominant stress which drives the crack.

The literature also contains important work that leads to better understanding of tire design and durability that are very close relation to tire belt separation. From the Joseph D. Walter's research on the cord-rubber composite material calculation [33], more detailed studies for calculating effective properties have been performed using strength of materials concepts [34,39], and by linear elasticity concept [35,36]. Farhad Tabaddor demonstrated using more refined traction boundary conditions [34], and pointed out the numerical values of transverse modulus for two-dimensional and three-dimensional case are very different. The equations for transverse modulus are:

$$E_2 = (\frac{E_m}{V_m}) / (1 - \nu_m^2) \tag{1.6}$$

for two-dimensional case, and

$$\frac{1}{E_2} = 2(\frac{\nu_m V_m}{1 - \nu_m} + \frac{\nu_f V_f}{1 - \nu_f})^2 / (\frac{E_m V_m}{1 - \nu_m} + \frac{E_f V_f}{1 - \nu_f}) \tag{1.7}$$

for the three-dimensional case. In this dissertation, Alfredo Balco de Morais's transverse modulus [39] was used for anisotropic analysis. He modeled the square cell, as seen in Figure 1.2, as cord division and rubber division, respectively. Applying the force equilibrium, boundary condition and Hooke's law, equation (1.8) can be derived. The advantage of this closed-form equation is that it does not need any empirical parameter. The final form is:

$$E_2 = \frac{\sqrt{V_f}}{\frac{\sqrt{V_f}}{E_{f2}} + (1 - \sqrt{V_f}) \frac{1 - \nu_m^2}{E_m}} + (1 - \sqrt{V_f}) \frac{E_m}{1 - \nu_m^2}. \tag{1.8}$$

Any purely analytical attempt to calculate the stress for lifetime prediction in a tire is facilitated based on the bodyline profile equation. The conventional tire contour design has been based on the natural profile theory [41,42] that upon inflating a tire, the body ply tension becomes uniform. But this approach does not guarantee all performance quality at the same time. The motivation, therefore, behind a tire contour design theory [43-46] is to make a new bodyline profile, which is intentionally modified from the natural bodyline profile, in order to

increase the tire durability, without sacrificing other important performance characteristics. A good representative design theory for a new bodyline is the Tension Control Optimization Theory (TCOT) [44-46] and Stress-Strain Cycle Optimization Theory (CSSOT) [43]. Tire lifetime was increased 10~15 % by adoption of new profile. The main comparison variables of finite element analysis are ply tension force, belt edge shear strain and crack length. The profile [46] that is chosen for this dissertation has a flatter tread radius than conventional tire, and it showed more durable from indoor and outdoor test results [46].

For more durable tire design, finite element analysis has widely been utilized in many fields. A passenger tire was analyzed using three-dimensional finite element method [47,48], which has three different belt structures to evaluate qualitatively the belt edge endurance. After De Eskinazi's works [47] on the utilizing of finite element to tire belt durability, some finite element applications were performed [49,50] for developing new belt constructions. Recently, rebar elements have been used instead of anisotropic constitutive modeling in composite layers [53-55]. The advantage of rebar element usage in a tire problem is that individual material property can be directly used for representation rubber and cord, respectively. In this study, both cases (rebar and anisotropic modeling) will be analyzed, and compared to determine which modeling is more reasonable for tire fracture analysis. A steady-state formulation of the rolling contact problem

was developed in [51]. This formulation enabled the study the tire characteristics when a tire is rolling under free rolling, traction, braking and cornering conditions.

1.3 Thesis Objectives

The objective of this thesis is to introduce methodology for prediction of the lifetime of a tire. The considerations needed for an energy release rate variation study to improve predictions of failure are divided into:

a) finite element type and composite material characteristics,
b) location of crack initiation and the direction of crack propagation,
c) mesh density in crack region,
d) analysis methodology and loading condition,
e) calculation of strain energy release rate for crack propagation,
f) determination of crack growth characteristics, and
g) lifetime prediction by combining J-integral and crack growth history.

This study assumes that an initial flaw exists inside the tire, in the suggested local model, due to a mechanical inhomogeneity caused during the manufacturing process. This study also considers how different driving conditions, such as free

rolling, braking, traction and lateral loading, contribute to the detrimental effects of belt separation in tire (size: 12R22.5) failure.

1.4 Thesis Presentation

This thesis is divided into eight Chapters. In Chapter II, general background to tire durability analysis, such as characteristics of cord-rubber composites, tire design theory and belt durability are re-examined. Chapter III describes modeling of materials. Constitutive equations for anisotropy and rubbery material are summarized. In Chapter IV, the key point for local modeling is suggested and the methodology for global-local analysis is discussed based on the three-dimensional finite element analysis. Different driving conditions also are clarified. Chapter V represents the theoretical relation of energy release rate and crack growth analysis. In Chapter VI, the computed J-integral solutions using suggested local crack model are evaluated to identify the effects of different crack sizes, different mesh densities, different driving conditions, and anisotropy in composite layers. In Chapter VII, the lifetime of a tire is calculated based on the J-integral values and closed form of integral equation. Finally, conclusion and recommendation for further works are summarized in the last Chapter.

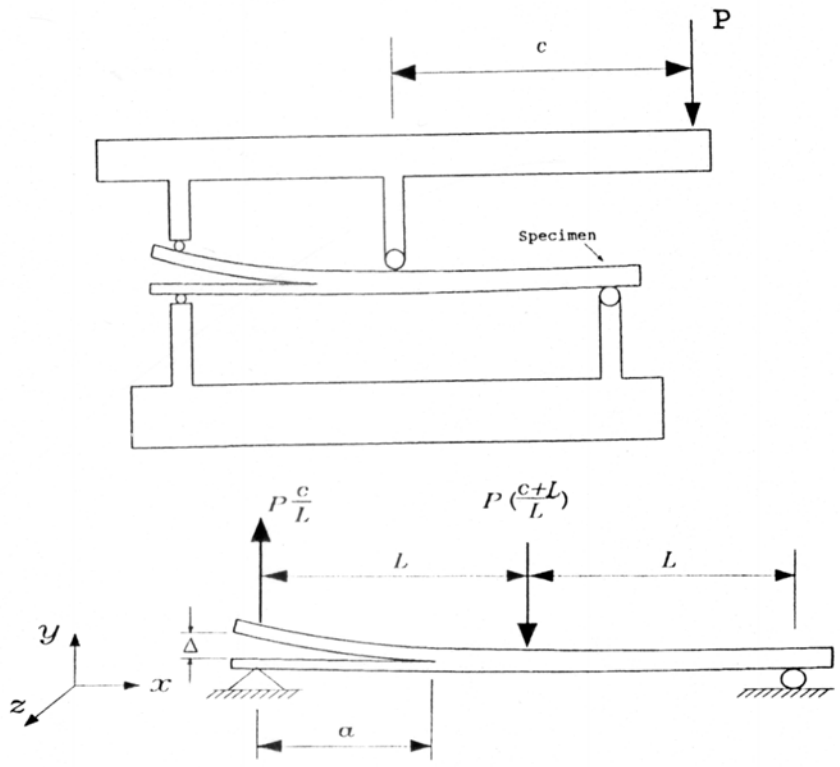

FIGURE 1.1 ─ Mixed mode bending specimen and test apparatus [22].

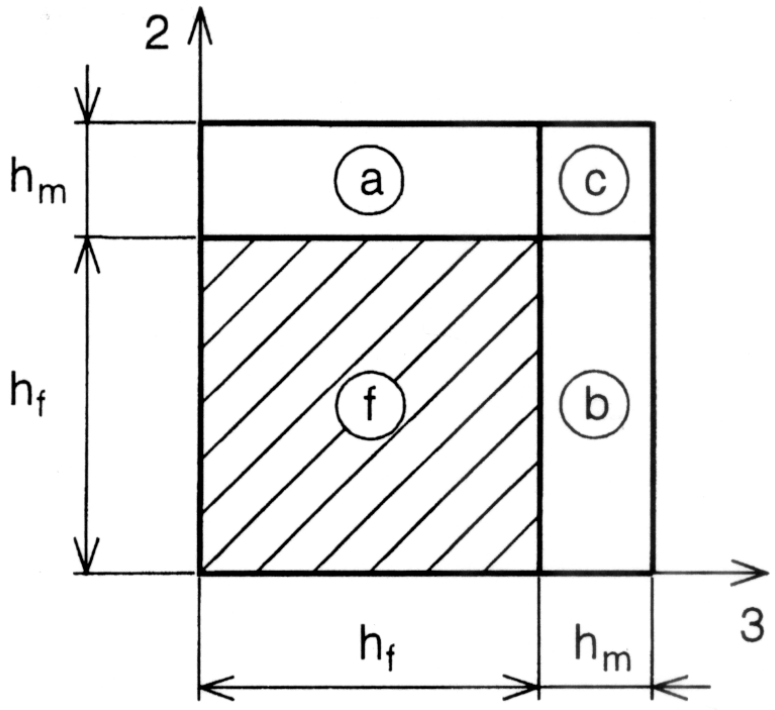

FIGURE 1.2 ─ The square cell and its subcells [39].

CHAPTER II

BACKGROUND TO TIRE DURABILITY

Tire durability is the most important metric in the design of a pneumatic tire. This chapter addresses the general background of tire durability. The background first discusses how characteristics of cord-rubber composites are used to understand durability in the presence of composite layers and, how these characteristics contribute to the physical analysis of tire belt durability. This background then briefly covers conventional tire design theory to emphasize the importance durability has in relation to tire profile and then discusses belt failure mechanism as motivation for durability analysis. The last section of this background presents the important role of fracture mechanics predicting lifetime of a tire using the finite element method.

2.1 Characteristics of Cord-Rubber Composites

The cord-rubber composites are the principal components in a pneumatic tire. The fundamental functions of the tire are to withstand the vehicle load and to transfer traction forces to the road surface. Tire composite characteristics provide structural integrity to support these main functions without sustaining damage. Therefore, understanding the cord-rubber composite characteristics is very

important in tire problems. Figure 2.1 represents the flow sequence of cord-rubber composite analysis. In general, the single cord-rubber composite layers, as shown in Figure 2.2, are considered linear orthotropic when referring to material axes. The strain-displacement relations are nonlinear due to geometric nonlinearities. For determination of the material properties in the cord direction and the perpendicular cord direction, the Halpin-Tsai equation [33] has widely been used. In recent years, rebar-elements [53-55] could be applied for individual reinforcing cords to represent uniaxial reinforcement in composite skims. The fundamental difference in both cases is in that how the composite material properties can be represented in the form of stiffness matrix. In this work both cases are introduced and compared to determine which one is better choice for tire fracture analysis. First, classical method for cord-rubber composite analysis is introduced and then, rebar-element concept is mentioned. The representative formula for anisotropic material properties in a single ply is of the Halpin-Tsai equation;

$$
\begin{aligned}
&E_1 = E_C V_C + E_R(1 - V_C) \\
&E_2 = E_R(1 + 2V_C)/(1 - V_C) \\
&G_{12} = G_R[G_C + G_R + (G_C - G_R)V_C]/[G_C + G_R - (G_C - G_R)V_C], \\
&\nu_{12} = V_R \nu_R + V_C \nu_C \\
&\nu_{21} = \nu_{12} \times E_2 / E_1
\end{aligned}
\qquad (2.1)
$$

where

$E_1 \equiv$ Young's modulus in a cord direction

$E_2 \equiv$ transverse Young's modulus

$G_{12} \equiv$ in-plane shear modulus

$\nu_{12} \equiv$ major Poisson's ratio

$\nu_{21} \equiv$ secondary Poisson's ratio

$E_C \equiv$ Young's modulus of cord

$E_R \equiv$ Young's modulus of rubber

$G_R \equiv$ shear modulus of rubber

$V_C \equiv$ volume fraction of steel cord in a single ply

And the remaining properties; $E_{3,}G_{13,}G_{23,}\nu_{13,}\nu_{23,}\nu_{31,}\nu_{32}$, can be calculated by reciprocal relations.

The general stress-strain relation in an elastic material can be represented by an equation for each stress and strain components of the from

$$\sigma_{ij} = \hat{E}_{ijkl}\varepsilon_{kl} \tag{2.2}$$

For the linear elastic material, matrix form of the three-dimensional orthotropic case is obtained by using stress and strain symmetry condition.

$$\begin{Bmatrix} \sigma_1 \\ \sigma_2 \\ \sigma_3 \\ \tau_{23} \\ \tau_{31} \\ \tau_{12} \end{Bmatrix} = \begin{bmatrix} C_{11} & C_{12} & C_{13} & 0 & 0 & 0 \\ C_{12} & C_{22} & C_{23} & 0 & 0 & 0 \\ C_{13} & C_{23} & C_{33} & 0 & 0 & 0 \\ 0 & 0 & 0 & C_{44} & 0 & 0 \\ 0 & 0 & 0 & 0 & C_{55} & 0 \\ 0 & 0 & 0 & 0 & 0 & C_{66} \end{bmatrix}, \tag{2.3}$$

where

$$\begin{aligned} &C_{11} = \frac{1-\nu_{23}\nu_{32}}{E_2E_3\Delta}, C_{22} = \frac{1-\nu_{13}\nu_{31}}{E_1E_3\Delta}, C_{33} = \frac{1-\nu_{12}\nu_{21}}{E_1E_2\Delta}, \\ &C_{12} = \frac{\nu_{21}+\nu_{31}\nu_{23}}{E_2E_3\Delta}, C_{13} = \frac{\nu_{31}+\nu_{21}\nu_{32}}{E_2E_3\Delta}, C_{23} = \frac{\nu_{32}+\nu_{12}\nu_{31}}{E_1E_3\Delta}, \\ &C_{44} = G_{23}, C_{55} = G_{31}, C_{66} = G_{12} \end{aligned} \tag{2.4}$$

and, $\Delta = \dfrac{1-\nu_{12}\nu_{21}-\nu_{23}\nu_{32}-\nu_{13}\nu_{31}-2\nu_{21}\nu_{32}\nu_{13}}{E_1E_2E_3}$

By assigning the angle β, counter-clock wise, from element axis, as seen in Figure 2.2, the stress transformation relation to element axis is

$$\{\sigma\}_{1,2,3} = [T]\{\sigma\}_{r,s,t}, \tag{2.5}$$

where $[T]$ is transformation matrix, and it has the following components.

$$\{T\} = \begin{bmatrix} \cos^2\beta & \sin^2\beta & 0 & 0 & 0 & 2\sin\beta\cos\beta \\ \sin^2\beta & \cos^2\beta & 0 & 0 & 0 & -2\sin\beta\cos\beta \\ 0 & 0 & 1 & 0 & 0 & 0 \\ 0 & 0 & 0 & \cos\beta & -\sin\beta & 0 \\ 0 & 0 & 0 & \sin\beta & \cos\beta & 0 \\ -\sin\beta\cos\beta & \sin\beta\cos\beta & 0 & 0 & 0 & \cos^2\beta-\sin^2\beta \end{bmatrix}. \tag{2.6}$$

By applying the transformation rule, an equation (2.5) can be expressed in terms of element strain.

$$\begin{aligned}\{\sigma\}_{r,s,t} &= [T]^{-1}\{\sigma\}_{1,2,3} = [T]^{-1}[C]\{\varepsilon\}_{1,2,3} = [T]^{-1}[C][T]^{-T}\{\varepsilon\}_{r,s,t} \\ &= [Q_{ij}]\{\varepsilon\}_{r,s,t}\end{aligned} \quad (2.7)$$

where $[Q_{ij}]$ is the modulus matrix referred to an element axis, and it's components are:

$$\begin{aligned}
Q_{11} &= C_{11}\cos^4\beta + 2(C_{12}+2C_{66})\sin^2\beta\cos^2\beta + C_{22}\sin^4\beta \\
Q_{12} &= (C_{11}+C_{22}-4C_{66})\sin^2\beta\cos^2\beta + C_{12}(\sin^4\beta+\cos^4\beta) \\
Q_{13} &= C_{13}\cos^2\beta + C_{23}\sin^2\beta Q_{16} = [C_{11}\cos^2\beta - C_{22}\sin^2\beta - \\
&(\cos^2\beta-\sin^2\beta)(C_{12}+2C_{66})]\sin\beta\cos\beta \\
Q_{22} &= C_{22}\cos^4\beta + 2(C_{12}+2C_{66})\sin^2\beta\cos^2\beta + C_{11}\sin^4\beta \\
Q_{16} &= [C_{11}\sin^2\beta - C_{22}\cos^2\beta + (\cos^2\beta-\sin^2\beta)(C_{12}+2C_{66})]\sin\beta\cos\beta \\
Q_{32} &= C_{13}\sin^2\beta + C_{23}\cos^2\beta \\
Q_{33} &= C_{33} \\
Q_{24} &= Q_{25} = Q_{34} = Q_{35} = Q_{46} = Q_{56} = 0 \\
Q_{36} &= (C_{13}-C_{23})\sin\beta\cos\beta \\
Q_{44} &= C_{44}\sin^2\beta + C_{55}\cos^2\beta = Q_{55} \\
Q_{45} &= -C_{44}\sin\beta\cos\beta + C_{55}\sin\beta\cos\beta \\
Q_{66} &= (C_{11}+C_{22}-2C_{12})\sin^2\beta\cos^2\beta + C_{66}(\cos^2\beta-\sin^2\beta)
\end{aligned} \quad (2.8)$$

Now consider two-ply layers ($\pm\theta$ plies), as shown in Figure 2.3 subjected to a longitudinal load, for obtaining analytic form of shearing strain. This two-ply

layer is representative of structure of the #2 and #3 belt of a typical truck tire. From the constitutive equation (2.7), we can obtain an analytical form of shear strain γ_{xz} [33] at each edge of the belt:

$$\gamma_{xz}\,|_{y=\pm b} = \varepsilon_x (2\cot^2\theta - 1)\,. \tag{2.9}$$

This relation implies the out of plane shear strain vanishes when the plies are oriented by $\theta = \pm 54.7^o$, and maximum value at cord angle 15°~20°. Shear strain as a function of cord angle for two plies that have opposite direction of cord angle is illustrated in Figure 2.4. From this result, the range of fundamental tire cord construction can be chosen to reduce or minimize the shear strain when a tire is inflated.

The original purpose of rebar-elements usage for composite layers is to calculate the material properties more in detail by defining cord and rubber separately, instead of average values when anisotropic formulations are used. Rebar-elements use a standard technique in the formulation of stiffness matrices for fiber and matrix. The final effective stiffness matrices consist of fiber and matrix parts together. Through a variational approach based on the potential energy, the global governing equation is [53-55]:

$$\widetilde{K}\Delta u = \widetilde{R}\,, \tag{2.10}$$

For further discretization of stiffness matrix into a rebar element with single fibers, n_{sf} and fiber layer, n_{fl} it leads to an element level:

$$K^{11} = K_m^{11} - \sum_{1}^{n_{sf}} K_m^{11sf} - \sum_{1}^{n_{fl}} K_m^{11fl} + \sum_{1}^{n_{sf}} K_s^{11fl} + \sum_{1}^{n_{fl}} K_{fl}^{11fl} , \qquad (2.11)$$

where

$$K_m^{11sf} = \iiint (B^T C_m B + G_m)'' J'' d\xi d\eta d\zeta . \qquad (2.12)$$

The other components of stiffness matrices may be represented by similar form, and described more detail in reference [53-55]. Rebar-elements, therefore, need an individual material property in conjunction with proper definition of cord angle orientation. The advantages of rebar elements for tire composite layers are individual material property may be used directly for input, and the cord angle change can be visualized from checking the model and analysis results. But there are limitations of rebar elements. When we need a heat transfer analysis for obtaining temperature profile inside of a structure or we need a coupled thermal-displacement analysis for studying the thermal effect, rebar element cannot be applied directly. For these we need a model that has separated elements, reinforced material and matrix, respectively or has an average values of material properties.

2.2 Tire Design Theory

The analysis of stresses and energies based upon the given tire profile (body line equation) is the first step for lifetime prediction in a tire, therefore

having an equation for the body line profile and surface curvature are the very beginning and the most important stage for tire development. The design variables such as belt skim dimension, material property and cord orientation are inter-related with each other and also related with tire profile. In other words, to improve tire durability, profile design is one of the most important design variables; without the modest profile no good performance can be guaranteed.

The conventional tire contour design has been based on the natural profile theory [41,42] that upon inflating a tire, the body ply tension becomes uniform. An equation that governs the natural body line is defined as:

$$y = \int_{\rho}^{\rho_o} \frac{(\rho^2 - \rho_m{}^2)\exp\int_{\rho}^{\rho_o}(\frac{\cot^2\alpha}{\rho})d\rho}{\sqrt{(\rho_o{}^2 - \rho_m{}^2)^2 - (\rho^2 - \rho_m{}^2)^2\exp 2\int_{\rho}^{\rho_o}(\frac{\cot^2\alpha}{\rho})d\rho}}, \qquad (2.13)$$

where, ρ is radius from tire axis to a point on the surface, ρ_m is radius from tire axis to a point of maximum sectional width, and α is the angle between cord element and a "parallel of latitude" on the tire. The assumptions in driving equation (2.13) are that steel cord support inflation pressure and rubber only plays a role to prevent air leakage, and a tire is assumed to be a net, with pin joints at the intersection of the cords. But this approach dose not satisfy all performance requirements at the same time, such as durability, tread wear, noise, rolling resistance, vibrations, and traction and handling.

The motivation behind a tire contour design theory is to make a new body-line profile, which was intentionally modified from the natural bodyline profile, in order to increase the tire durability without sacrificing other important performance characteristics. Good representative design theories for a new body line are the TCOT [44-45] and CSSOT [43]. The tire design theories, which have so far developed, mainly rely on the indoor or field test to demonstrate the improved performance. Fracture analysis for lifetime prediction using a finite element analysis is a superior tool to other tests for reduction of tire design process.

The profile introduced in this research for lifetime prediction was chosen from three candidates [46] that represent different ratio of section height. This profile represented lower stress concentration at the belt edge, and showed longer mileage than other conventional tires.

2.3 Belt Durability

Tire belt durability is characterized by the initiation of failure at the belt edge region, and propagation of this failure into the interior until the ply is separated. The typical failure types that include belt separation are cord failure, rubber failure, or adhesive failure between cords and rubber. The main reason of service failure in the belt edge region is rubber cracking caused by stress

concentration from the material discontinuity and large deformation when a tire is rolling. A good typical example of belt edge crack for a radial tire is shown in reference [11][1].

From past to present, many researches have been performed to increase belt durability using experimental and numerical methods. The key points for durability increase are consists of two topics:

1. How the stress concentration in the belt edge can be reduced?
2. What criterion can effectively explain the belt durability?

The first of these topics is related to design variable analysis, represented in reference [46-50]. The second part of these governs the durability index, and it can be used as quantitative comparison for different design variables. Representative examples for this are interply shear strain [46-48], strain energy density [46,47], cracking energy density [28], energy release rate [7,10,11].

Fracture mechanics analysis has emerged as very powerful tool for evaluation of belt durability, and lifetime prediction from the D.C. Prevorsek's experimental study [2] on a tire. There were two main difficulties in application of analytical fracture mechanics to a tire. Where and which type do the belt separation occur (inter-laminar: fracture mode type)?. Secondly how the mixed-

[1] This reference was obtained from on-line, www.ce.berkeley.edu/~sanjay/

mode could be expressed in terms of analytical forms. The two-dimensional model [5,7] or isotropic beam model [22] were preferred for numerical analysis or analytical approach. By introducing finite element based fracture mechanics, it is possible to predict not only for lifetime but an evaluation of durability.

There are many factors affect tire deformation shape when a tire is rolling, such as an inflation pressure, vehicle load and vehicle speed. The details of the effects of main factors are illustrated in reference [11]. In this research constant inflation pressure, constant vehicle velocity and vehicle load are assumed.

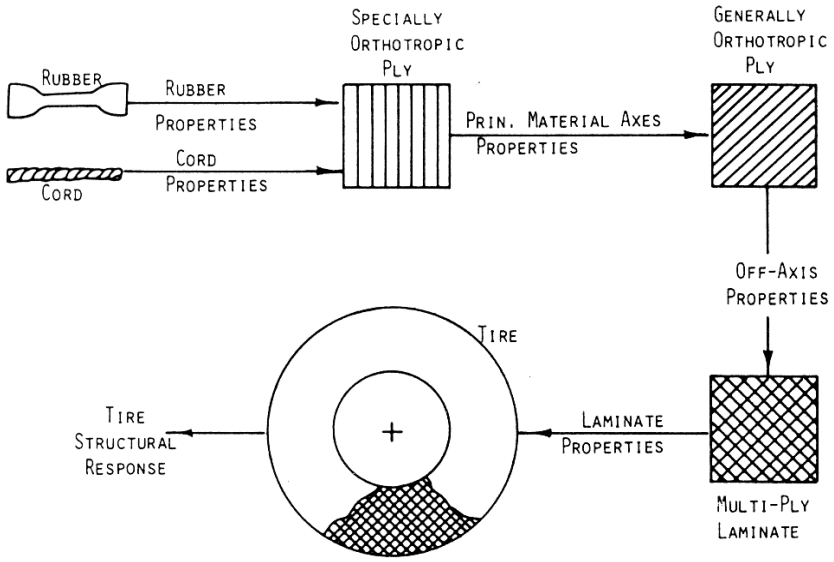

FIGURE 2.1 — Flow chart of cord-rubber composite analysis [33].

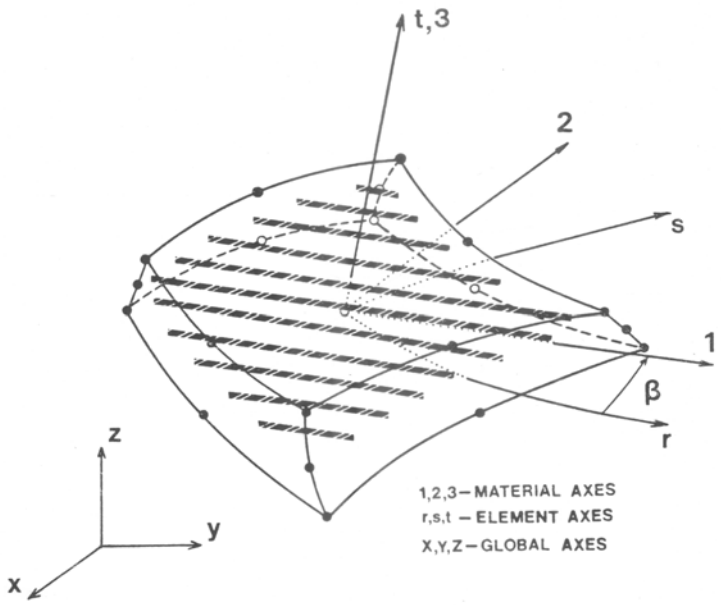

FIGURE 2.2 – Three-dimensional cord-rubber composite element [52].

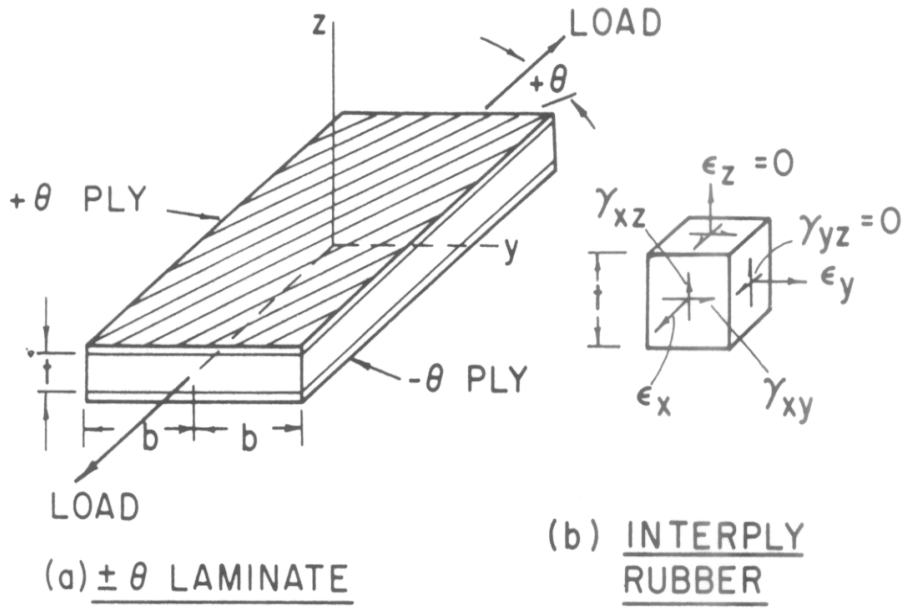

FIGURE 2.3 — Model interply deformations [33].
(a) $\pm\theta$ laminate subjected to longitudinal load
(b) resulting strains on interply rubber

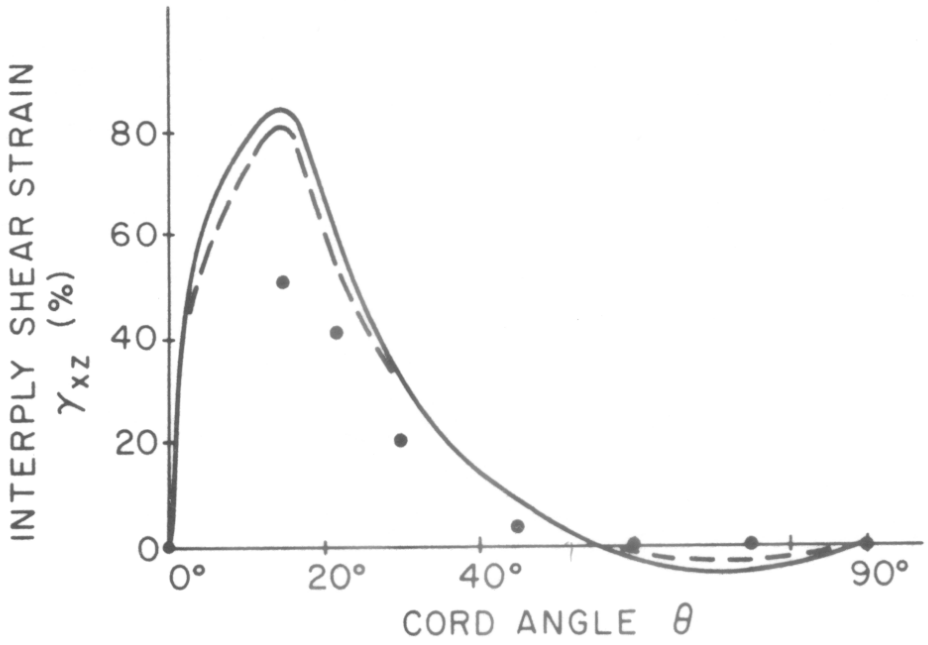

FIGURE 2.4 — Shear strain γ_{xz} as a function of θ, theoretical predicted (—, ----) and experimentally measured (•) for polyester-rubber laminate at 10% specimen extension [33].

CHAPTER III

MODELING OF MATERIALS

This chapter presents the formulation of the models used to represent the physical elements of a pneumatic tire. The first section gives the form of the equilibrium equation to the pneumatic tire for the specific application of predicting the lifetime of a tire. The second section describes the constitutive equation for representing an anisotropic material in the tire model. The third section describes the constitutive equation for rubber-like material represented in the tire model. Both of these descriptions formulate the incorporation of true pneumatic tire characteristics into the simplified tire model.

3.1 Equilibrium Equation

The equations governing the distribution of stresses may be derived from linear and angular momentum principles. The principal of linear momentum at each particle, with surface area A and volume V, is

$$\int_A TdA + \int_V fdv = \int_V \rho \ddot{u} dV \ , \qquad (3.1)$$

in which T is the traction vector; f is body force vector; ρ is the mass density in the reference configuration; and superimposed dots indicate time rate. If we

assume the stresses are C^1 continuous then, equation (3.1) leads to an equilibrium equation:

$$\sigma_{ij,j} + f_i = \rho \ddot{u}_i . \tag{3.2}$$

For static problems, the right hand side term of equation (3.2) is zero. The principal of angular momentum at each particle, with distance r from initial configuration to reference configuration, is

$$\int_A (r \times T) dA + \int_V (r \times f) dV = \int_V (r \times \rho \ddot{u}) dV . \tag{3.3}$$

The relation between traction vector and deformation gradient is, by applying the stress symmetry condition from principal of angular momentum:

$$TF^T = FT^T , \tag{3.4}$$

where, F is the deformation gradient tensor.

3.2 Constitutive Equation for Anisotropic Material

The general constitutive equation for anisotropic linearly elastic composite materials can be represented as

$$\sigma_{ij} = \hat{E}_{ijkl} \varepsilon_{kl} , \tag{3.5}$$

in which σ_{ij} is the Eulerian stress tensor, $\hat{E}_{ijkl}$ the fourth-order anisotropic elasticity tensor, and ε_{kl} the Almansi strain tensor. To define the anisotropic

elasticity tensor for cord-rubber composites, the symmetry condition of stress and strain, mentioned in the section 3.1, is needed. Equation (2.7) shows the general anisotropic elasticity tensor. In a tire problem, the transverse effective property, E_2, has important meaning, since the tire cords experience a large bending effect during contact. The belt edge-cushion rubber experiences a large shear deformation in a circumferential direction. Thus, three-dimensional states of stress and strain must be considered. As originally given the Halpin-Tsai form of the stress-strain equations relate to states of plane stress only. Therefore, direct application of the Halpin-Tsai equations to a tire problem is not recommended. In this research, a more analytical expression, equation (3.6) which was developed by solid mechanics background [39], is combined with the Halpin-Tsai equations:

$$E_2 = \frac{\sqrt{V_C}}{\frac{\sqrt{V_C}}{E_C} + (1-\sqrt{V_C})\frac{1-\nu_R^2}{E_R}} + (1-\sqrt{V_C})\frac{E_R}{1-\nu_R^2}. \qquad (3.6)$$

3.3 Constitutive Equation for Rubber-like Material

Elastomers used in tires act as almost incompressible materials since bulk modulus of rubber is greater than Young's modulus. In other words, the volume of rubber components changes very little although elastomers undergo very large elastic deformations. The strain energy potential defines hyperelastic materials, its

use ignores any internal energy dissipation associated with the deformation process: It ignores hysteresis and the Mullins effect [28]. The Mullins effect is not important in tires because the material response becomes stable (repeatable) after a few cycles of loading. The hysteresis is small compared to the stored energy and is important only in the calculation of rolling resistance. The strain energy potential depends on the current state of deformation only. When the body we are concerned which is subjected to the motion shown in Figure 3.1, every material point such as P is moved to a new position. The motion of each point is described by a smooth mathematical function called the deformation function. The mathematical notation designated by two sets of Cartesian coordinates x_i and X_i with $i = 1,2,3$, called initial coordinates and final coordinates respectively, that denote the undeformed and deformed positions of the body, is

$$x_i = x_i(X,t), \tag{3.7}$$

which gives the present location x_i of the particle that occupied the point (X_1, X_2, X_3) at time t=0. The deformation function x defines the motion of every material particle. This description of deformation expressed by equation (3.7) is called the Lagrangian formulation. Alternatively, one may express the undeformed configuration in terms of the deformed configuration:

$$X_i = X_i(x,t), \tag{3.8}$$

which leads to the Eulerian description of continuum. An important variable in the characterization of deformation of the nonlinear continuum mechanics is the deformation gradient, F:

$$F = \frac{\partial x}{\partial X}. \tag{3.9}$$

The deformation gradient maps an infinitesimal element in the reference configuration into the current configuration. From the deformation gradient we know the following important meanings:

1. The deformation gradient contains all information necessary to reproduce the deformation in a locality.
2. It knows nothing about the translation. It does know about rigid body rotation.
3. Naturally, it knows about the stretching in its own neighborhood.
4. It is fundamental for kinematic analysis of the deformation.

In general, the body may translate, rotate and distort and/or stretch. In order to distinguish the straining part of the motion from the rigid body rotation, we may apply very useful factorization for the deformation gradient, polar decomposition. There are two ways in representing polar decomposition: A stretch of dX followed by a rotation, or a rotation of dX followed by a stretching:

$$\begin{aligned} F &= RU \\ F &= VR \end{aligned}, \qquad (3.10)$$

where R is the pure rigid body rotation matrix, and it has orthogonal property. U and V both matrices have positive definite and symmetry properties. For the sake of convenience, we use $C(=U^2)$ as appropriate arguments of Σ. If the material is isotropic in the undeformed configuration then, instead of being a function of the components of C, the energy density can be written as a function of the three principal scalar invariants of C:

$$\begin{aligned} I_1 &= tr(C) = C_{11} + C_{22} + C_{33} \\ I_2 &= \frac{1}{2}(tr(C)^2 - tr(C^2)) \\ I_3 &= det(C) = (det(F))^2 \end{aligned} \quad . \qquad (3.11)$$

The principal invariants are the coefficients in a cubic equation, the characteristic equation of matrix C, whose roots are the squares of the principal stretches.

$$-(\lambda^2)^3 + I_1(\lambda^2)^2 + I_2(\lambda^2) + I_3 = 0 . \qquad (3.12)$$

This equation (3.12) implies that the invarients determine the stretches and visa versa. Then we write, in general,

$$\Sigma = \Sigma(\lambda_1, \lambda_2, \lambda_3) . \qquad (3.13)$$

The determination of Σ in terms of three principal stretches is a difficult task. Valanis and Landel proposed a simple form with assuming separable stretches:

$$\Sigma(\lambda_1, \lambda_2, \lambda_3) = w(\lambda_1) + w(\lambda_2) + w(\lambda_3) . \qquad (3.14)$$

R.G. Ogden, [56], suggested a particular form for the function $w(\lambda)$ in the Valanis-Landel formulation.

$$w(\lambda) = \sum_{i=1}^{n} C_i(\lambda^{\alpha_i} - 1). \tag{3.15}$$

This algebraic form of Ogden's model is well chosen in that quite reasonable curve fits to material test data can be obtained with *n=2* or *3*. In ABAQUS the following equation (3.17) for Ogden's model is used, and considered compressibility parameter D_i .

$$\Sigma = \sum_{i=1}^{N} \frac{2\mu_i}{\alpha_i^2}(\overline{\lambda}_1^{\alpha i} + \overline{\lambda}_2^{\alpha i} + \overline{\lambda}_3^{\alpha i} - 3) + \sum_{i=1}^{N} \frac{2}{D_i}(J^{el} - 1)^{2i}, \tag{3.16}$$

where $\overline{\lambda}_i = J^{-1/3}\lambda_i$; $\overline{\lambda}_i$ is the deviatoric principal stretches; J^{el} is an elastic volume ratio; N is a material parameter; and μ_i, α_i, and D_i are temperature-dependent material parameters. The particular material models: Mooney-Rivilin; neo-Hookean can also be obtained by controlling material parameters. With an input of test data, the material parameters μ_i, α_i, and D_i can be automatically calculated. In this research, nominal stresses and strains via uniaxial test were used.

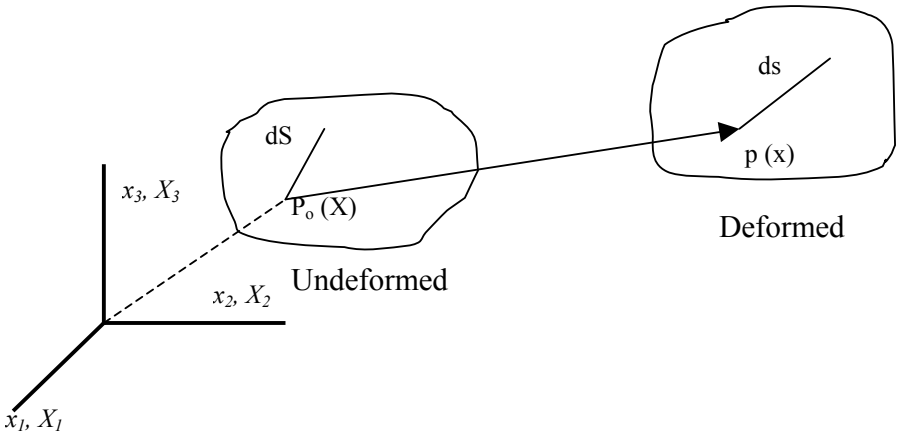

FIGURE 3.1 — Displacement vector in Cartesian space.

CHAPTER IV

FINITE ELEMENT MODELING

A finite element modeling approach is used to predict the lifetime of a tire. This modeling technique provides a detailed description of the stresses, energies, and deflection of a tire. This modeling technique is based on the viewpoint that the mechanical behavior of the pneumatic tire is correlated to its deformation resulting from the elastic and geometric properties of the carcass and inflation pressure. This chapter presents a description and the benefits for using a global-local modeling, an FEM approach, with respect to durability prediction. Furthermore, this section discusses the application and use of steady-state rolling analysis to determine tire durability.

4.1 Global-Local Modeling

A global model consists of quadratic continuum brick elements. The global model, shown in Figure 4.1, can be automatically generated from the two-dimension axisymmetric model (Figure 4.2), which considers full cross section for analysis of rolling condition in conjunction with lateral loading. In addition to full cross section with a quadratic element type, the global model contains very small segments (0.18 deg.) in a circumferential location where fracture model will

be considered. In other words, small segments are imbedded at the specifically designated region: top part; 90 deg.; 140 deg.; 160 deg.; 166 deg.;, and contact center part. Inflation, contact and rolling analysis can be performed using this three-dimensional full model. Composite layers (belts or body ply) are represented as two different types: rebar elements; anisotropic composite elements. For a validation of the global analysis, load-deflection response is compared with experimental values in Figure 4.3, and two different section types (full and symmetric) considering two different types of composite layers are examined. The important results inferred from this Figure are:

1. Finite element results show a little overestimate of material stiffness.
2. More reasonable result is obtained when rebar elements are used instead of an anisotropic material property for composite layers.
3. No significant difference was found between symmetric and full model.

There are many outputs available from the global analysis such as velocity profile of cross section, interlaminar shear strain and footprint, etc., but all other outputs are ignored in here.

Local crack modeling is very efficient as it can obtain detailed information on the stresses, and energies in the local region that has negligible effect on the overall solution, all the while allowing for the reduction of computing time. With a connection of time-dependent values of variables to the relevant boundary nodes of the local model, only one local model is needed for a tire problem to obtain the solution in any location of circumferential direction. Therefore broad-based analyses are possible in the vulnerable regions such as, belt edge, bead turn-up, pattern block analysis and so on.

An important aspect of this study is to identify the appropriate local model for fracture mechanics analysis in a tire belt separation problem. The local crack model suggested in this research has the following key features:

1. the model may represent the direction of crack propagation,
2. the model may show the fracture modes (deformation modes) at any regions along circumferential directions of a tire by introducing small element segments that are aligned in a circumferential direction in the global model,
3. the model may has a close relation with the global model without loss or jumps in interpolation of boundary conditions, by introducing fine

meshes in the local model and small element segments that are aligned in a circumferential direction in the global model,

4. the model has zero singular points in numerical sense, since it has sufficient smoothness in crack front node sets, and
5. the model is simple in modeling for variation of mesh density and crack size.

As mentioned in the previous section, the main cause of failure in the belt edge region is stress concentrations that are induced by material discontinuity and large cyclic-deformation under service. We, therefore, need to investigate particularly the state of stresses in the belt edge crack tip. From the global analysis results, for instance static contact problem, the state of stress in the belt edge element is represented in Figure 4.4 and with numerical data Table 4.1. The coordinate axes introduced in Figure 4.4 have same direction of the real tire representation, meridian, radial, and circumferential direction. The detailed observation of the state of stresses, as seen in Table 4.1, gives the following important features:

1. An element at the 2nd belt edge is subject to normal compression stresses in a meridian and radial direction, and by normal tension stresses in a circumferential direction.
2. The values of normal stresses are relatively small to other components, but the shear component resulting on the plane 1~2 or 1~3 is the largest value.
3. The component of shear stresses resulting on the plane 2-3 is small relative to the normal stress component.

The above features imply that plane 2-3 acts like a symmetry plane, as shown in Figure 4.5. One might argue from this observation how tire belt separation will occur, having with compression stresses and shear stresses components. This phenomenon might microscopically be understood by the fact that a small initial flaw existing in the local region causes the beginning stage of the damage. In general the rapidity with which the transition from localized to global damage relies on the stress distribution, as well as the material property. A cyclic loading of a tire induces large amount of shear stresses as mentioned above, therefore, these values have large effects on a tire separation problem. Equation (4.1) shows the spherical and deviator stress components.

$$\sigma_{ij} = \delta_{ij}\sigma_{kk} / 3 + S_{ij}, \qquad (4.1)$$

in which

$$\delta_{ij}\sigma_{kk} / 3 = \sigma_M \,, \tag{4.2}$$

where, σ_M is the mean normal stress. The deviator stress tensor is,

$$\{S_{ij}\} = \begin{bmatrix} S_{11} & S_{12} & S_{13} \\ S_{21} & S_{22} & S_{23} \\ S_{31} & S_{32} & S_{33} \end{bmatrix} = \begin{bmatrix} \sigma_{11} - \sigma_M & \sigma_{12} & \sigma_{13} \\ \sigma_{21} & \sigma_{22} - \sigma_M & \sigma_{23} \\ \sigma_{31} & \sigma_{32} & \sigma_{33} - \sigma_M \end{bmatrix}. \tag{4.3}$$

The tearing of the material is not unaffected by the spherical stress but related to the stress or strain that is independent of spherical stress; deviator stress. This reasoning is why belt separation will occur from the combination of normal and shear stress in a tire problem.

A symmetry model that has a rectangular type of crack surface, however, can cause a singular problem at the sharp corner crack fronts or can give misleading solutions. Therefore, a cylindrical local crack model that has a circular crack surface inside is suggested to overcome the numerical difficulties arising when rectangular type of crack surface is adopted instead of circular type. This is important background why cylindrical local model was chosen for calculation of energy release rate in a tire problem. Of course, adjusting the diameter of an initial flaw existing inside the cylinder can control the crack size.

4.2 Steady-State Rolling Analysis

A steady-state transport scheme is applied for rolling analysis, and different driving conditions such as free-rolling, braking, traction, and lateral loading are considered. The expression for a tire rigid body rotation is described as Eulerian and deformation as Lagrangian description. With the utilization of this kinematical relation, the steady contact problem is converted into a purely spatially dependent problem. Therefore fine mesh is confined only near the contact region. The steady-state transport analysis needs the traveling straight-line velocity of tire axle, v_o, and tire spinning angular velocity, ω, to characterize the driving condition. For a straight line rolling, a velocity and acceleration in an arbitrary point *P* of a tire is expressed by v_0 and ω, since a tire is rolling under planar motion.

$$\begin{aligned} \vec{v}_P &= \vec{v}_0 + (\vec{\omega} \times \vec{r}_{P/o}) \\ \vec{a}_P &= \vec{\omega} \times (\vec{\omega} \times \vec{r}_{P/o}) \end{aligned} . \qquad (4.4)$$

Classification of driving conditions depend on the sense of torque and a given vehicle angular velocity. The range of an angular velocity might be estimated by equation (4.5), with the dimension of the free radius of a tire, r, and distance from the rim center to the contact point of a rigid surface, H, when the tire is deflected.

$$\frac{v_o}{r} < \omega < \frac{v_o}{H} . \qquad (4.5)$$

From this relation, the range of the angular velocity for a free rolling tire is around 57.4~61.2 radian/second. The free rolling condition can be determined from the torque vs. angular velocity curve, or from the circumferential deformation shape. We find it to be 59.3 radian/sec. in case of traveling velocity 70 mph.

Most of the time a tire experiences steady-state rolling. On a flat surface the tire undergoes the combined load effects as shown in Figure 4.6. The loads are vehicle weight force (W); friction force (F_f); dynamic force (F_d); and tire inertia force (F_i). The dynamic force F_d means the force transmitting from the vehicle suspension movement, upward and downward, to a tire. Therefore the effect of dynamic force could be ignored with assuming of tire rolling on a flat surface of rigid body, and of little effect it has on the tire relative to other forces such as weight and friction force. Under these typical load conditions, the tire will experience a large deformation, and this cyclic large deformation can cause a separation that will begin at the belt edge region.

Some conditions are assumed in this research to describe the lateral loading effect of steady-state rolling condition. First, vehicle travels without slip, along the radius R circle, and secondly, vehicle travels with constant velocity (constant angular velocity) without tip over. In other words, vehicle is traveling under the critical condition, without slip and tip over. Third, no slip angle is considered. We have to decide the lateral load F_f or lateral displacement. A

Figure 4.7 shows the vehicle system which simplifies the. In Figure 4.7, M means the vehicle mass, F_c the centrifugal force exerted on the center of mass of a vehicle, F_f the frictional force induced on a tire footprint, α the angular acceleration, and F_f the lateral load that exerted on foot area of a tire. The vehicle (double-axle) travels on the ramp (radius: 30m), and the speed and weight are 70mph, 10ton. The dimensions assumed of vehicle system are: B=2.5m; H=3.5m; b=1m; h=2m. From the Newton's 2nd law (4.6), the lateral force may be obtained analytically. It is about 5240N. We can estimate the lateral displacement corresponding to this analytical lateral force by the experimental curve of the lateral load-deflection. The lateral displacement corresponding to the lateral force 5240N is 60mm. This value is applied on the contact patch to give boundary condition.

$$\begin{aligned} &\sum F_x = ma_x : -F_c - F_f = Ma_x \\ &\sum F_y = ma_y : F_N - Mg = 0 \\ &\sum M_{c.m} = I_{c.m}\alpha : F_f h - F_N b = I_{C.M}\alpha , \end{aligned} \tag{4.6}$$

The reader is cautioned about the purpose of this lateral loading analysis. It is not to describe the detailed description of the contact patch but to study general trend in fracture mechanics analysis by simplified assumption. If more detailed analysis is required of lateral loading, we have to study the relation between the effect of friction coefficient variation and lateral load.

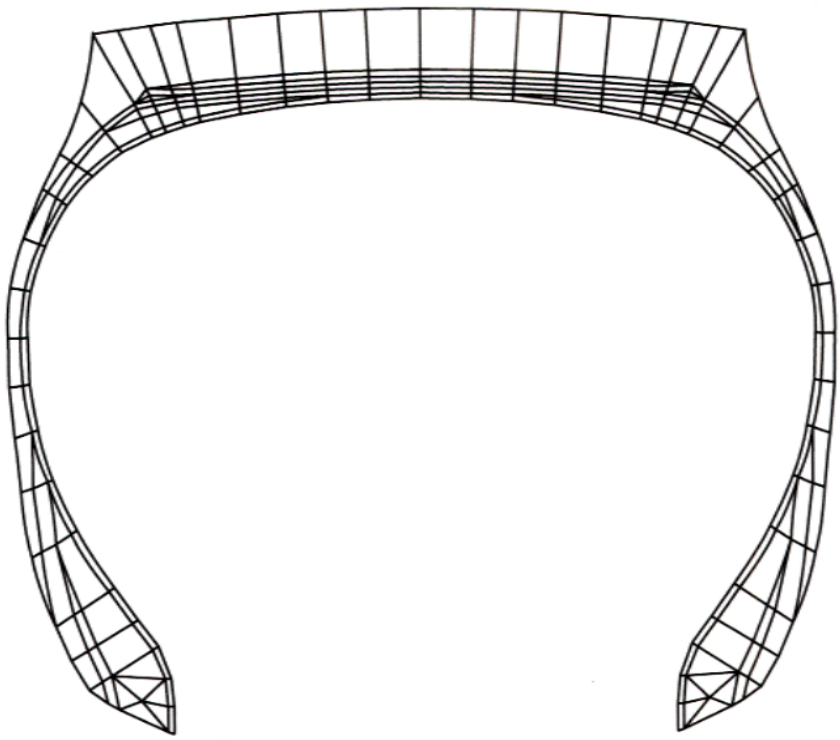

FIGURE 4.1 ─ Cross sectional two-dimension finite element model.

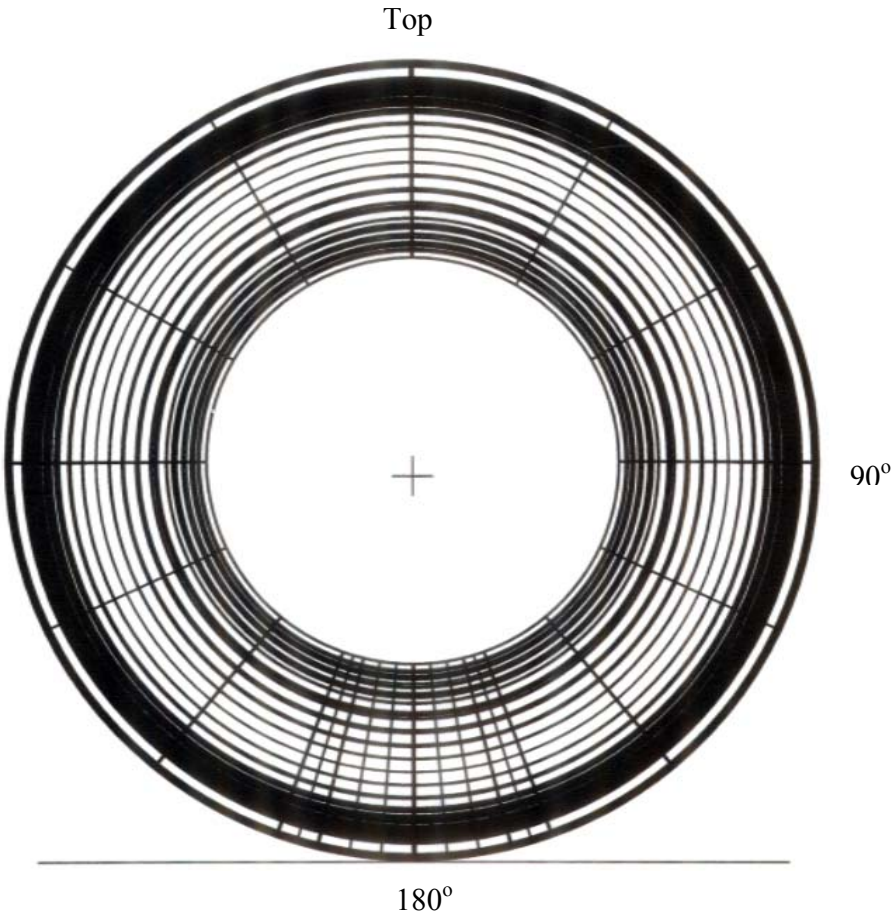

FIGURE 4.2 ─ Three-dimension finite element model.

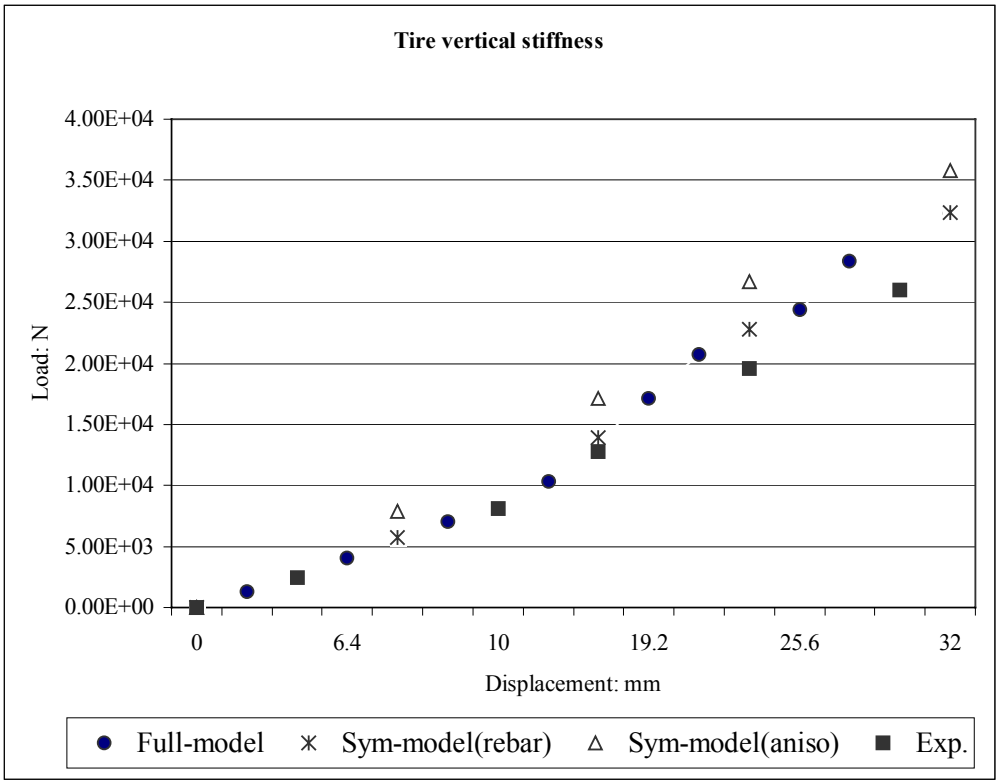

FIGURE 4.3 ─ Load-deflection curve.

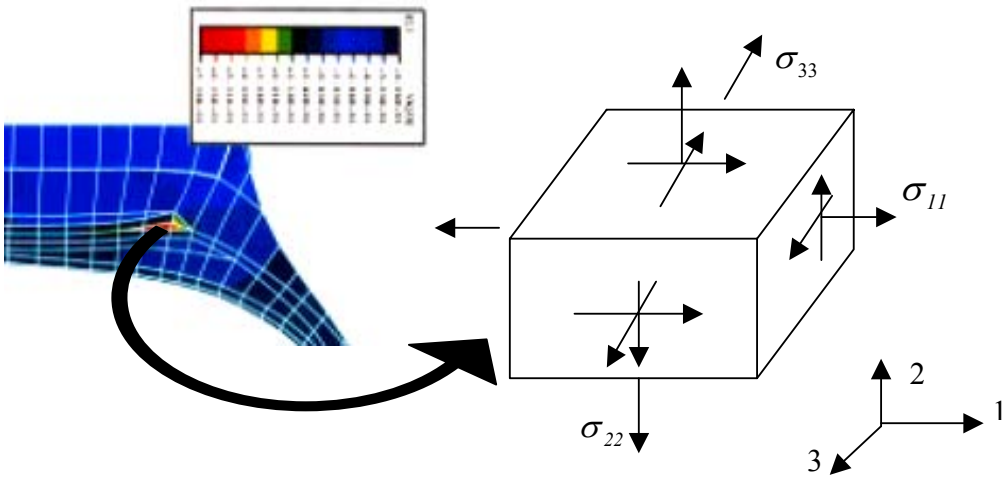

FIGURE 4.4 ─ State of stress for static contact at the belt edge region.
(1: Meridian direction, 2: Radial direction, 3: Circumferential direction)

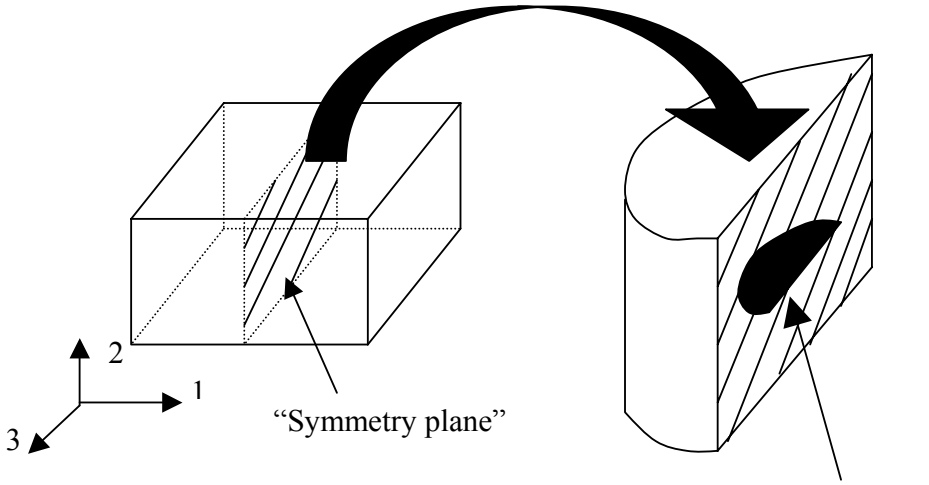

1: Meridian-direction
2: Radial-direction
3: Circumferential-direction

FIGURE 4.5 ─ Simplified symmetry model.

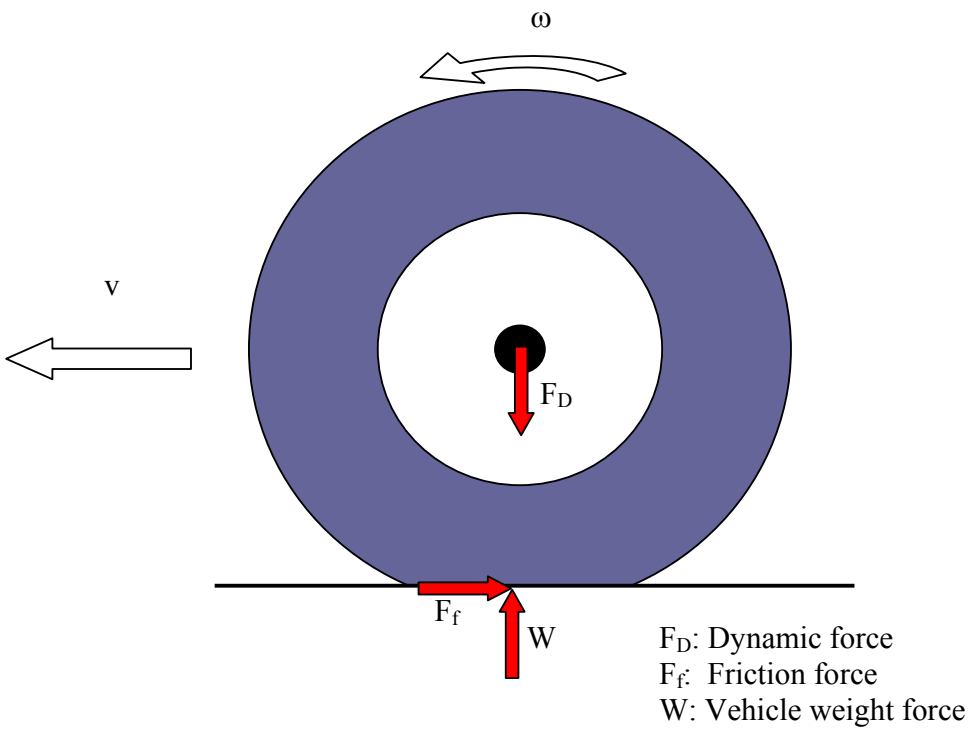

FIGURE 4.6 ─ Combined loads for steady-state rolling.

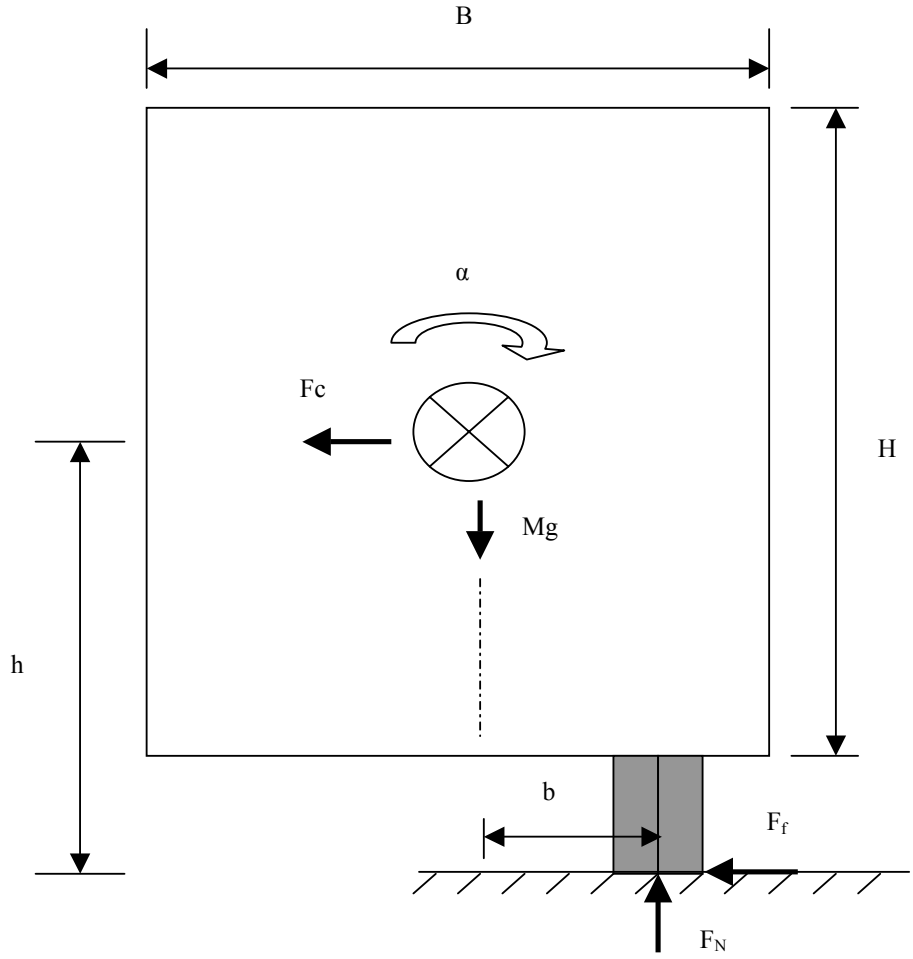

FIGURE 4.7 ─ Force equilibrium in a rolling tire.

TABLE 4.1 — State of stress for different driving conditions at the contact region.

Unit: N/m^2	σ_{11}	σ_{22}	σ_{33}	σ_{12}	σ_{13}	σ_{23}
Static - Contact	-3.5e+5	-2.7e+5	1.0e+5	1.0e+5	8.5e+4	8.0e+5
Free rolling	-3.3e+5	-2.7e+5	1.6e+5	1.0e+5	7.9e+4	7.8e+5
Traction	-3.4e+5	-2.7e+5	1.4e+5	1.0e+5	9.0e+4	7.9e+5
Braking	-3.2e+5	-2.5e+5	1.9e+5	1.1e+5	5.7e+4	7.6e+5

CHAPTER V

FRACTURE MECHNICS ANALYSIS

The following chapter describes how fracture mechanics can be used to predict the lifetime of a tire. The chapter first discusses the energy release rate plays in facilitating the calculation of a crack growth in the tire rubber component. Subsequently, the second part of this chapter discusses how a crack growth analysis can determine the lifetime of a tire through energy release rate calculation.

5.1 Energy Release Rate

In the fracture mechanics approach by finite elements, the energy approach (J-integral) is more powerful than point matching approach (stress intensity factor) for a tire problem, since energy approach can be applied for both linear and nonlinear material problem. In addition, the process of crack growth is often described in terms of energies. If the total energy balance of a body containing an initial flaw is considered, then the details of how the energy is distributed is not important. Griffith utilized this concept in the very first work in fracture mechanics. In a stressed body, the growth of the crack resulted in a decrease in the total energy of the body and that if this is greater than that

absorbed by forming the new crack surfaces, then the crack growth would be unstable. In other words, crack will grow if the energy available to create a unit area of crack growth is sufficient to overcome the material resistance. Energy release rate is frequently called a driving force or crack extension force, since it is also characterized by the derivative of potential energy.

$$G = -\frac{\partial PE}{\partial a}, \tag{5.1}$$

where PE is the potential energy, G is the energy release rate, and a the crack area. The negative sign is used since a reduction in system energy results in an increase in energy available for external work. In the absence of body forces the potential energy of the body, for two-dimensional elastic body shown in Figure 5.1, is

$$PE(a) = \int_A W dA - \int_{\Gamma_T} T_i u_i ds, \tag{5.2}$$

where W is the strain energy density, T_i are the traction vector components, u_i are the displacement vector components, and Γ_T denotes the contour of the body which the tractions are prescribed. For a hyperelastic material, the strain energy density function takes a specific functional form

$$W(\varepsilon) = \int_0^{\varepsilon_{ij}} \sigma_{ij} d\varepsilon_{ij}, \tag{5.3}$$

where σ_{ij} and ε_{ij} are the stress and strain tensors, respectively. Investigations of energy release rate for non-linear material, especially for rubber, have been

performed by Rivlin and Thomas [15]. In computational mechanics, energy release rate is used as same meaning of the *J*-integral, by conservation of the contour integral theorem. Rice [14] presented a path-independent contour integral, denoted *J*. The same definition holds for non-linear elastic materials. The value of *G* can be determined by the *J* integral.

$$G = J \equiv \int_{\Gamma} (W n_1 - T_i \frac{\partial u_i}{\partial x_1}) ds \qquad (5.4)$$

for a 1-direction crack case in the absence of body forces and thermal strains. To be path-independent of *J*-integral, equation (5.4), material must be homogeneous and elastic in the direction of crack propagation. Therefore, careful consideration is needed for an interfacial crack analysis. There are important considerations that how *G* is calculated in finite element analysis for rubber.

1. Form of strain energy density is used in the energies, i.e. Mooney-Rivlin or Ogden type etc. In this research, as mentioned in Chapter 3, Ogden type of strain energy density function is used.
2. *J*-integral is defined for contours in planes perpendicular to crack front and values vary along front. Therefore fine meshes and smooth crack fronts are required in the vicinity of crack region.

3. *J*-integral is path-independent. So the data used to calculate can be taken along contours away from singularity. Integral is calculated as domain integral over elements adjacent to contour.

In this research, no singular elements are used in the local model because of the large strain at the belt edge region. The contact condition subjected to two crack surfaces might allow the penetration of a master surface into a slave surface with the option of small sliding, since the crack mode is not a self-similar but a mixed-mode shape. Penetration in the real calculation did not in fact happen from the mode shapes.

Failure criteria for a mixed-mode fracture, like a tire separation problem, the maximum energy release rate and maximum tangential stress criterion are generally used. The maximum energy release rate criterion states that the crack will begin to propagate in the direction that maximizes the energy release rate, that

$$G \geq G_c, \tag{5.5}$$

where G_c is a material property and is a measure of the energy necessary to form new surfaces. This criterion does explain the only necessary condition but no sufficient condition for fracture, since it must be satisfied only if fracture occurs.

5.2 Crack Growth Analysis

A tire has many potential failure regions such as the groove, belt and bead. But most failures, which result in severe accidents, come from the belt separation due to large stress concentrations induced by material discontinuity in a macro-sense. An existing initial flaw at the belt edge rubber causes crack growth that is slow, stable or rapid according to the level of stress concentrations present. For repeated loadings the change in G during one cycle of loading is ΔG:

$$\Delta G = G_{max} - G_{min} . \qquad (5.6)$$

Assuming that G_{max} and G_{min} are the largest and smallest energy release rates among the results obtained for different positions, in circumferential direction, during rotation, ΔG can be calculated for one revolution. Repeated loadings that have values of ΔG less than the critical values G_c, each produces a very small but finite amount of crack growth. The rate at which a crack front advances is taken to be a function of ΔG. The dependence of rate of crack growth, $\frac{dc}{dN}$, on ΔG for a typical rubber is shown in Figure 5.2. In the region of stable crack growth the data are well described by a single power law.

$$\frac{dc}{dN} = A(\Delta G)^m , \qquad (5.7)$$

where c is the crack length in the unstrained state, N is the number of load cycles, and A and m are material parameters. Material parameters in this research were referred from the test data [11], shown in Figure 5.2.

The rate of crack growth depends not only on ΔG but also the ratio $R = \frac{G_{min}}{G_{max}}$. This can be represented by the various curves shown in Figure 5.3. Table 5.1 shows the energy release rate with respect to different driving conditions. From this table we can obtain the ratio, $R \cong 0.06 \sim 0.07$ when G_{min} is the value of inflation analysis results and G_{max} for rolling analysis results. But this point is still arguable in that which value of G_{min} is suitable for representing the real tire situation. In general, the slope of crack growth rate vs. energy release rate is steeper as R increases even though the critical energy release rate is same. Combining equations (5.6) and (5.7), it is possible to predict the total lifetime of a tire, in number of cycles. All possible driving conditions for a rolling tire will be considered in order to observe the condition that has the dominant effect on the peak energy release rate. To validate the local crack model, suggested in the present study, two variables (crack size and mesh density) are chosen, and applied to each driving condition for comparison.

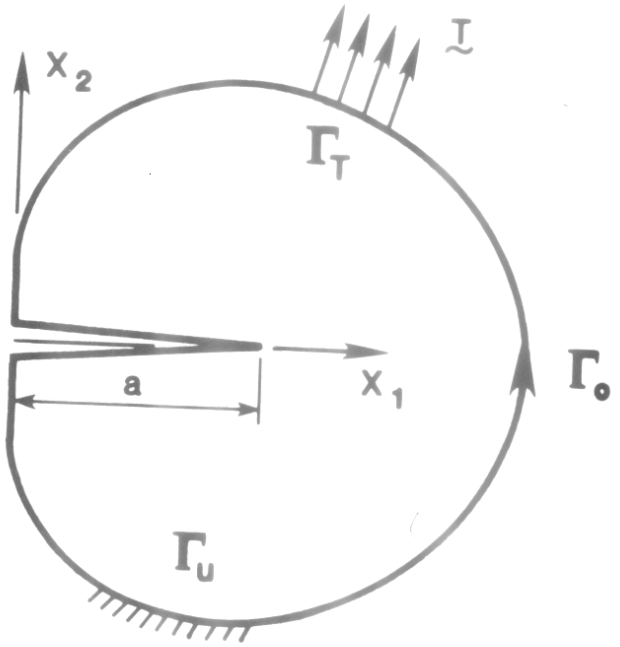

FIGURE 5.1 — A plane, cracked nonlinear elastic [57].

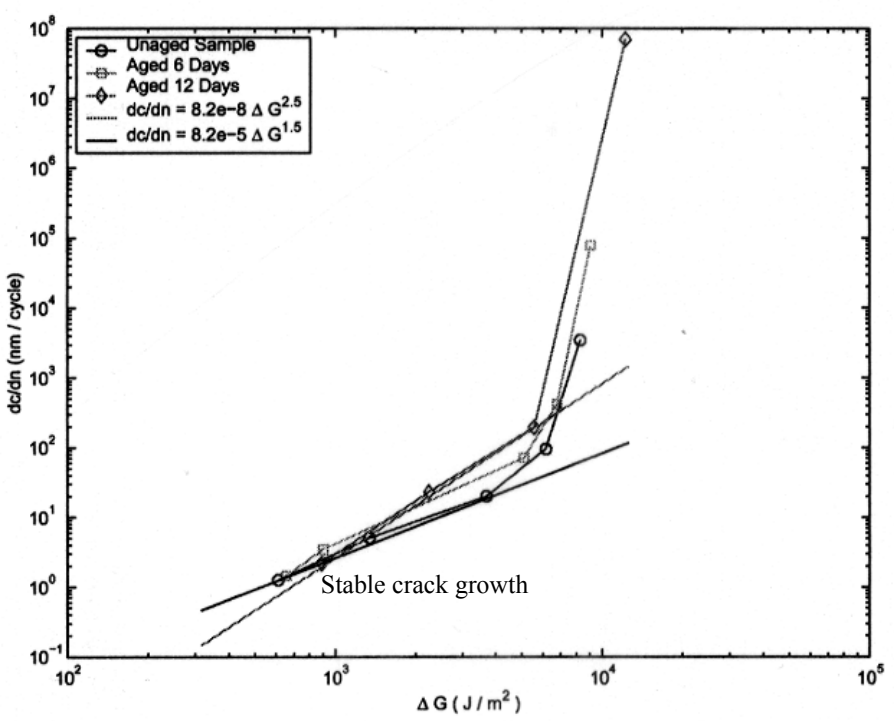

FIGURE 5.2 ─ Cut growth curves for belt edge rubber in unaged, 6 days aged, and 8 days aged conditions [11].

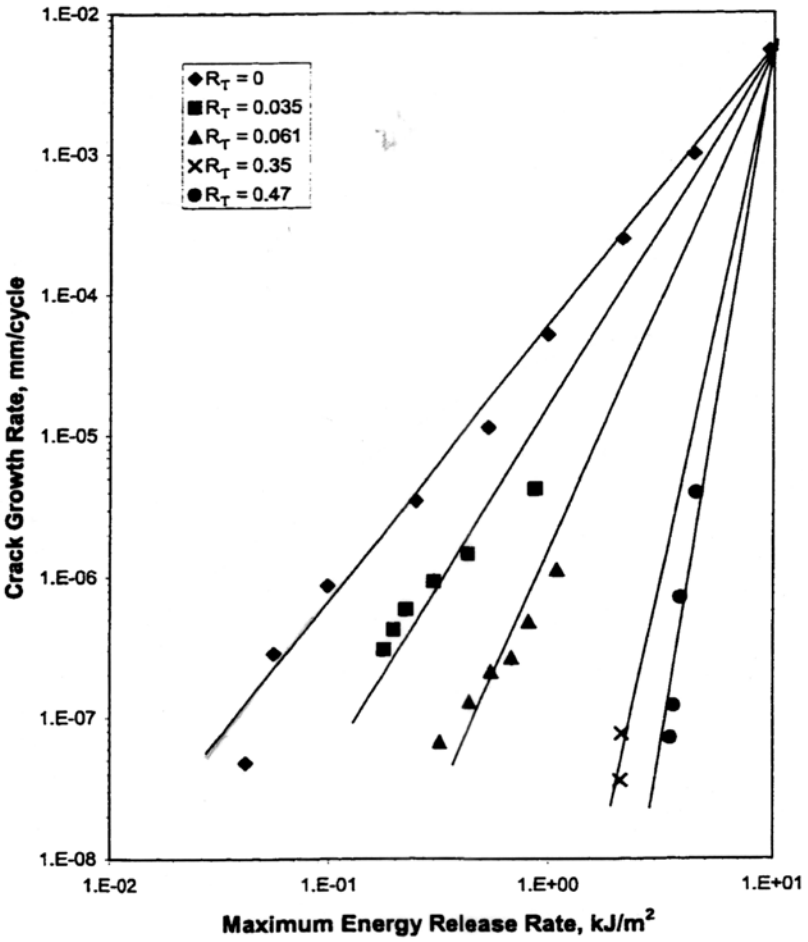

FIGURE 5.3 ─ The effect of R ratio on fatigue crack growth rate in gum NR [28].

TABLE 5.1 — Energy release rate with respect to different driving conditions.

Unit: J/m^2	G_{max}	G_{min}	ΔG		G_{max}	G_{min}	ΔG
Static contact				Free rolling			
. Small-crack	145	1(9)*	144	. Small-crack	140	1	139
. Mid-crack	198	2(14)	196	. Mid-crack	193	2	191
. Large-crack	285	4(22)	281	. Large-crack	273	4	269
. Critical-crack	10K	25	9975	. Critical-crack	10K	29	9971
Traction				Braking			
. Small-crack	143	1	142	. Small-crack	150	1	149
. Mid-crack	195	2	193	. Mid-crack	212	2	200
. Large-crack	281	5	276	. Large-crack	292	4	288
. Critical-crack	10K	26	9974	. Critical-crack	10K	25	9975

( )*: inflation

CHAPTER VI

APPLICATION AND J-INTEGRAL VALUES

This chapter takes the computed J-integral values and represents the suggested local crack model. The local crack is formed using a displacement boundary condition in a global model analysis in the presence of an initial flaw of circular shape. The first section presents the effect a crack size change has to an energy release rate. The second and third sections, respectively, examine the effect of a mesh density change and a material change to the local crack model. The last section describes how the J-integral values can represent different driving condition.

6.1 Crack Size Effect

In order to evaluate the effects of the different crack size on the energy release rate, three different crack sizes are chosen (Diameter: 1.5, 2.6, 4.8mm). The limitation of maximum size of the crack is restricted to the dimension of the local crack model, since the local crack model was generated to be located inside the belt edge rubber. Figure 6.1-6.3 show three local crack models, which have a different crack size depending on the mesh type: regular; doubles-mesh. These local crack models were generated using the real dimension of belt edge element.

The J-integral results with respect to a different crack size at the contact center region (180^o) for different driving conditions are represented in Figure 6.4 and Figure 6.5, which represent a regular-type and a doubled-type of mesh density respectively. From these figures, we can figure out the followings.

1. Energy release rate increases as crack size increases.
2. Energy release rate in the circumferential direction is higher than that of the meridian direction.
3. Energy release rate in the circumferential direction, of the braking case, shows the largest value among all other cases even though there are not big differences.

If the critical tearing energy of rubber components in a real tire can be assumed around 10 KJ/m^2 [11], as shown in Figure 5.2 for unaged, 6 day aged, and 8 day aged conditions, the critical crack length may be estimated by polynomial curve fit of the J-integral results. In almost all cases, shown in the Figure 6.4 and Figure 6.5, the slope of the J-integral curve is the same for all rolling conditions. The critical crack length is found to be about 23mm, by using a polynomial curve fit from Figure 6.4. However, it remains to be arguable whether or not the size of the initial flaw assumed in this research is valid with respect to the size induced by

manufacturing process. This leads to the question “can the critical length obtained from cylindrical symmetric model represent the average crack length?” To answer this question, considerable testing (indoor, lab and outdoor) and data acquisition are required.

Alternatively, an initial flaw can be measured by a holographic technique or approximated by a simple relationship between critical length and the shape factor only if the critical length and geometry related to an applied load are known. The obtained critical crack size is found to be valid from reference [12], which explains catastrophic failure when the crack length is slightly over 20mm.

6.2 Mesh Density Change

To study the effect that mesh density has on energy release rates in the local crack model, two different types of mesh densities are introduced for each crack size, regular-mesh and doubled-mesh. The typical examples are shown in Figure 6.1-6.3 for different crack size. The total number of elements for a regular-mesh and a doubled-mesh set up is listed in Table 6.1. The J-integral value should be path-independent for any chosen contours. It thus indicates mesh quality by virtue of the derivation of equation (5.11), from the conservation theorem and no singular points inside the contours. Figures 6.6-6.10 represent the J-integral value of small crack size with respect to a different mesh density for inflation analysis

and different driving conditions such as static contact, traction, braking and free rolling case, respectively. Figures 6.11-6.15 represent the J-integral value of middle crack size value with respect to a different mesh density for inflation analysis and different driving conditions such as static-contact, traction, braking and free rolling case, respectively. Figures 6.16-6.20 represent the J-integral value of large crack size with respect to a different mesh density for inflation analysis and different driving conditions such as static-contact, traction, braking and free rolling case, respectively.

When a tire is inflated (Figures 6.6, Figures 6.11 and Figures 6.16), the energy release rate shows the same value throughout any location in a circumferential direction for both types of mesh densities. The difference of J-integral values between each mesh density for same direction is reduced when the crack size increases. When a tire is loaded and rolling (Figures 6.7-6.10, Figures 6.12-6.15, Figures 6.17-6.20), no variation in the energy release rate was found from the top to just ahead of contact region (located at 140 deg.), and energy release rate increases linearly from a possible contact zone to the contact center point. In almost all cases, the energy release rate sharply increases in a circumferential direction compared to a meridian direction.

6.3 Driving Condition Change and Mode Shape

Driving conditions considered in this study are free rolling, traction and braking, in order to understand how different driving conditions contribute to the detrimental effects of belt separation in tire failure. As mentioned above, only small variation of J-integral values was found to each different driving condition for both circumferential and meridian directions.

Figures 6.21-6.25 represent the J-integral values of regular-type for inflation and different driving conditions such as static-contact, traction, braking and free rolling, respectively. Figures 6.26-6.30 represent the J-integral values of doubled-type for inflation and different driving conditions such as static-contact, traction, braking and free rolling, respectively. From these figures, no big variation was found for each different driving condition, except for the inflation case.

Figure 6.31 shows an opening mode at the top location, focused only for upper and bottom contact elements, when a tire is under the braking condition. At the contact region (180 deg. from top part), a combined mode (opening, tearing and sliding) was obtained, as shown in Figure 6.32. The same mode shapes were obtained in all other driving conditions. These two modes imply: a mixed mode is dominant in the contact region; opening mode is dominant in the top location.

This indicates tire belt separation in the belt edge region is highly related to the mixed deformation from the cyclic rotation of a tire.

When a lateral loading is applied simultaneously for a rolling tire through a contact patch like a Figure 6.33, the energy release rate shows a little higher than the cases of other rolling. The J-integral values for both directions of a regular mesh type are compared in Figure 6.34 and Figure 6.35 respectively, with other boundary condition types: static contact; static contact+lateral loading; braking; braking+lateral loading. From this comparison, we can figure out the energy release rate, for braking combined with lateral loading case, increases from top part as go along to a circumferential direction, and the value is larger than for just static-lateral loading applying. Of course, the J-integral value was compared at both part (a) and (b), Figure 6.33, to choose more vulnerable region. Part (a) shows higher values in J-integral.

6.4 Anisotropy in Composite Layers

To demonstrate the effect of the constitutive relation for an anisotropic elastic composite material, the modified Halpin-Tsai equations, as explained in chapter 3, are used. A large difference in the energy release rate was found, as seen in Figure 6.36, for large crack and regular mesh type in a circumferential between rebar and anisotropic case. When the composite layers are modeled as an

anisotropic constitutive relation, the peak value of energy release rate is considerably smaller than the use of rebar element. From this Figure 6.36, we can presume that the cord angle change at the belt edge is very sensitive to composite material properties, and it serves very large effect on the J-values. The cord angle change is related to the strain energy density calculation, especially for the local crack model. Therefore, the effect of a cord angle change should be considered to obtain more exact value of the energy release rate for the anisotropic material properties.

6.5 Summary of the energy release rate

A summary of the energy release rate with respect to different driving conditions is as follows.

1. Inflation analysis (P=830 kPa, Figures 6.6, Figures 6.11 and Figures 6.16):
    a. Doubling the mesh in the crack region reduced the difference of the energy release rate in the circumferential and meridian directions.
    b. Higher values of energy release rate were obtained in a circumferential direction than in the meridian direction.

2. Static contact, traction, free-rolling and braking analysis (Figure 6.22-6.25, Figure 6.27-30):

   Regardless of the different crack sizes and driving conditions,

   a. Energy release rate increased linearly at the location of 140^{o} from the top part.
   b. Higher values of energy release rate were obtained in the circumferential direction than in the meridian direction.
   c. Opening mode is dominant at the top region, and mixed-mode is dominant in the contact region.

3. Lateral loading analysis (Figure 6.34~6.35):

   a. Higher values of energy release rate were obtained in a circumferential direction than in the meridian direction.
   b. Energy release rate increase from top going in a circumferential direction.
   c. Higher values of energy release rate were obtained than that of the static-contact lateral loading case.

4. Anisotropy in composite layers (Figure 6.36):
    a. The peak value of energy release rate at contact center point is considerably smaller than the use of rebar element.
    b. Higher values of energy release rate were obtained in a circumferential direction than in the meridian direction.
    c. In general a tire is operating of the 0.4kJ/m^2 [11], it means the rebar modeling is more reasonable than anisotropic case.

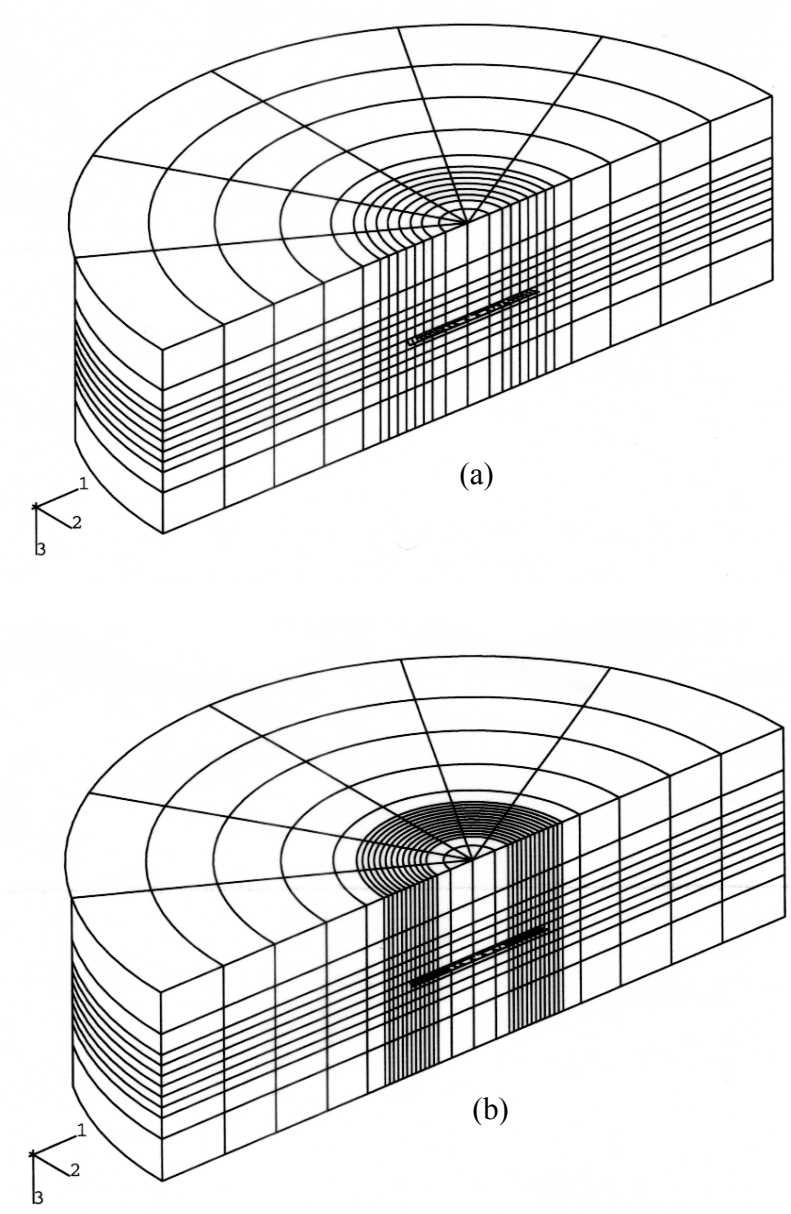

FIGURE 6.1 ─ Local crack model for small crack size.
(a) regular mesh type; (b) doubled mesh type

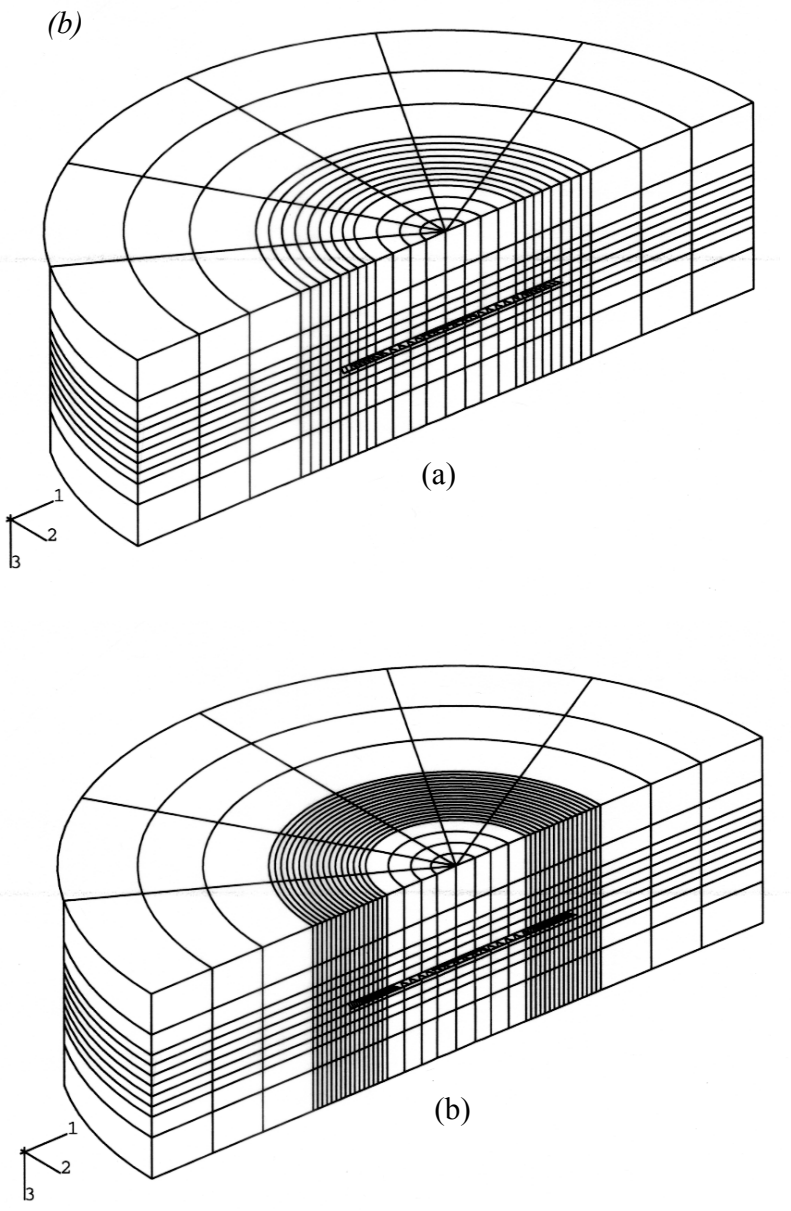

FIGURE 6.2 ─ Local crack model for middle crack size.
(a) regular mesh type; (b) doubled mesh type

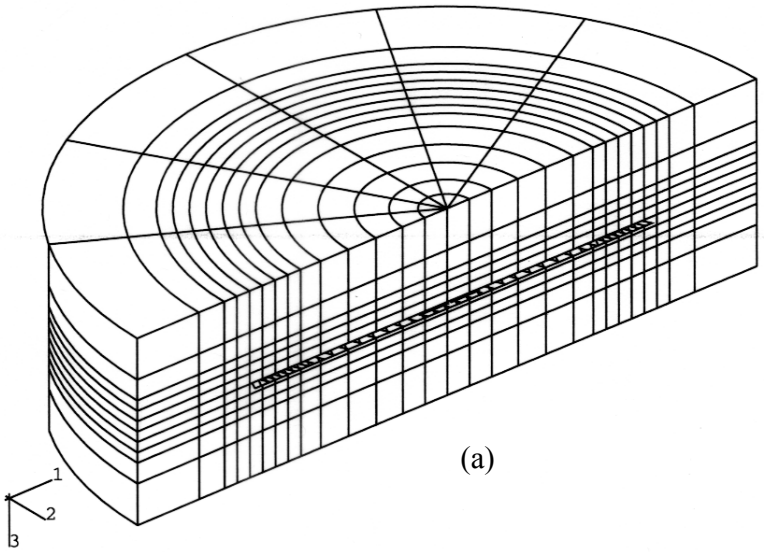

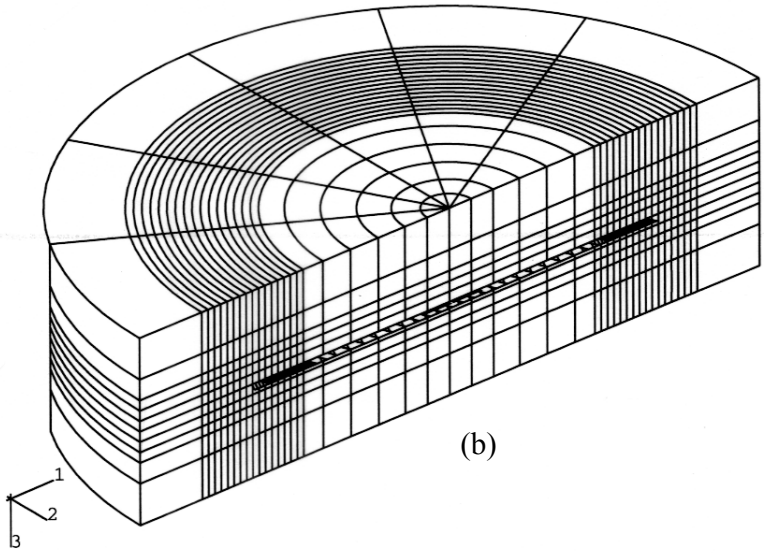

FIGURE 6.3 ─ Local crack model for large crack size. (a) regular mesh type; (b) doubled mesh type

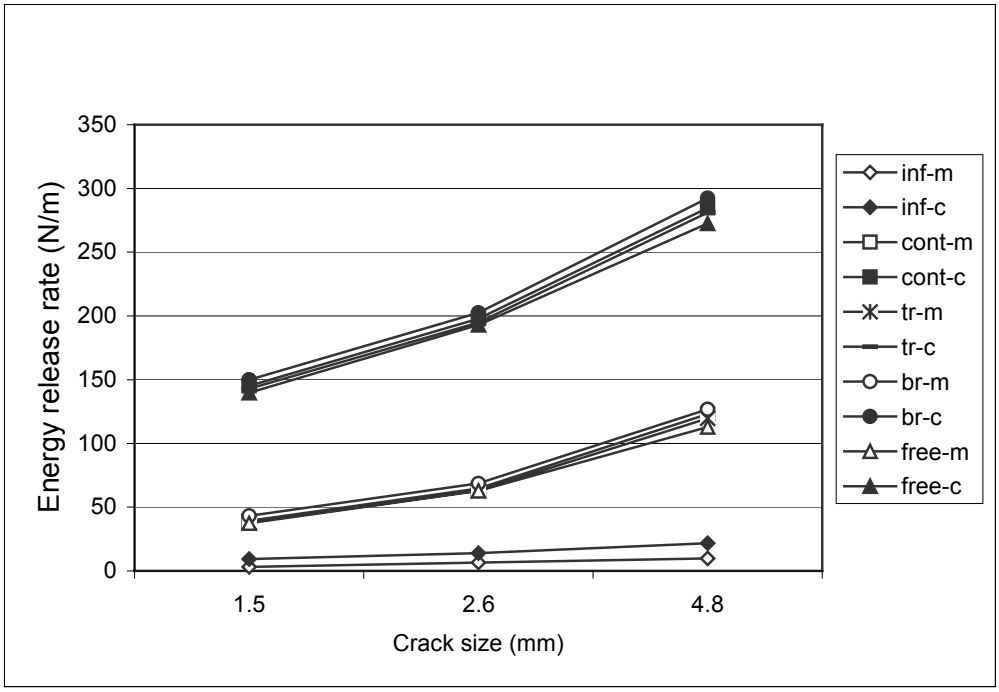

FIGURE 6.4 — J-integral with respect to different crack sizes for regular mesh type (inf: inflation, cont:static contact, tr: traction, br: braking, free: free-rolling, m: meridian direction,c: circumferential direction).

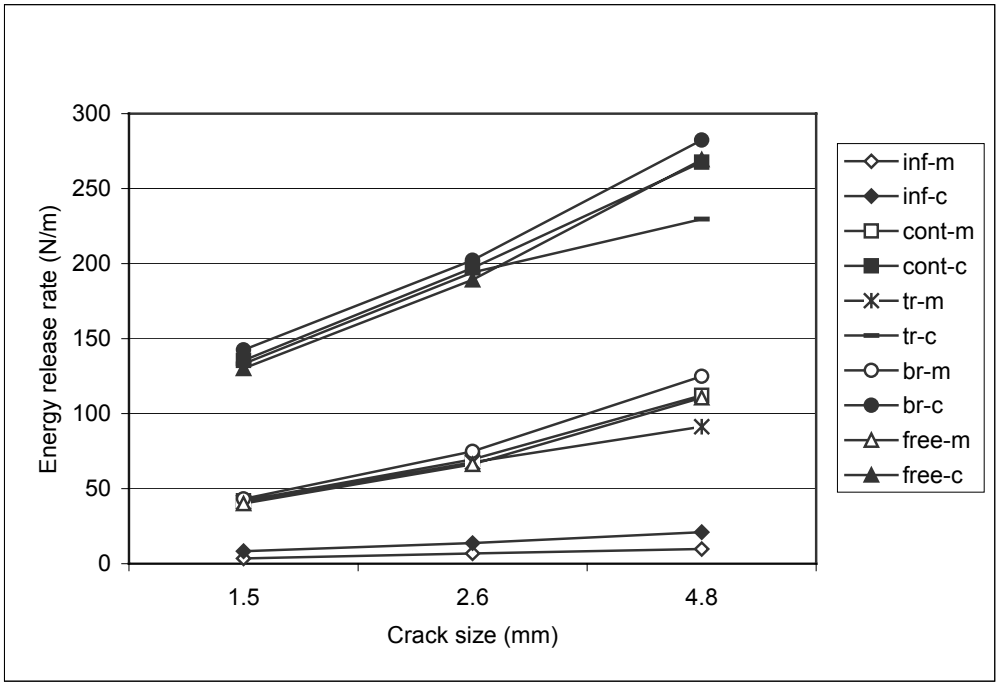

FIGURE 6.5 — J-integral with respect to different crack sizes for doubled mesh type (inf: inflation, cont:static contact, tr: traction, br: braking, free: free-rolling, m: meridian direction,c: circumferential direction).

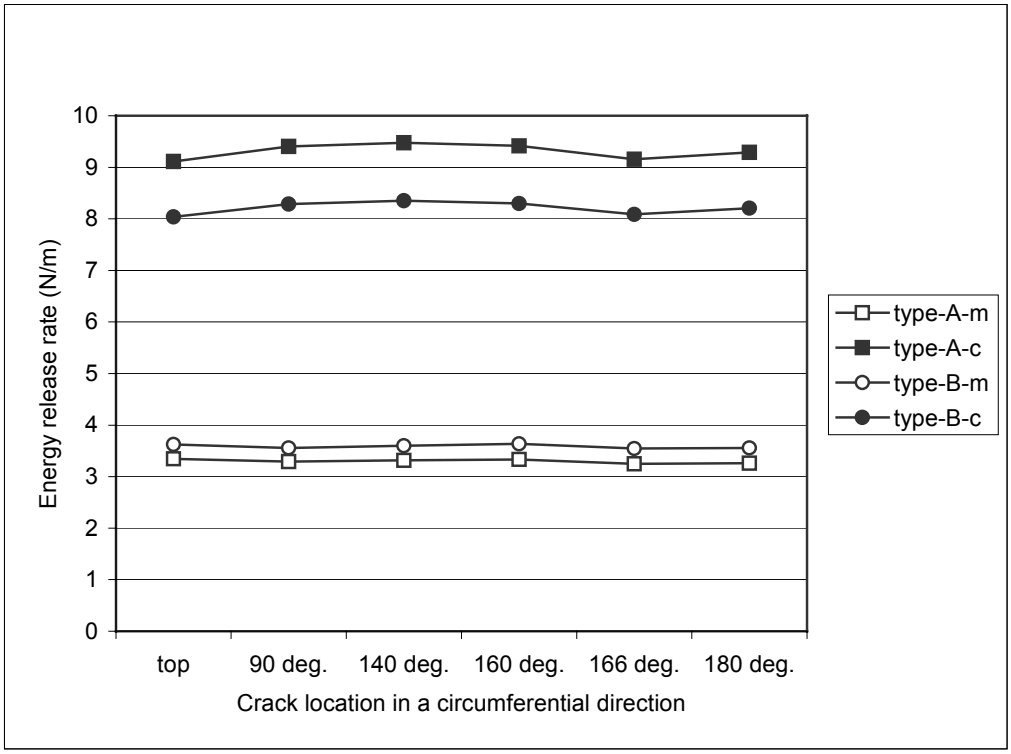

FIGURE 6.6 ─ J-integral with respect to different mesh density for inflation analysis of small crack (type-A: regular mesh, type-B: doubled mesh).

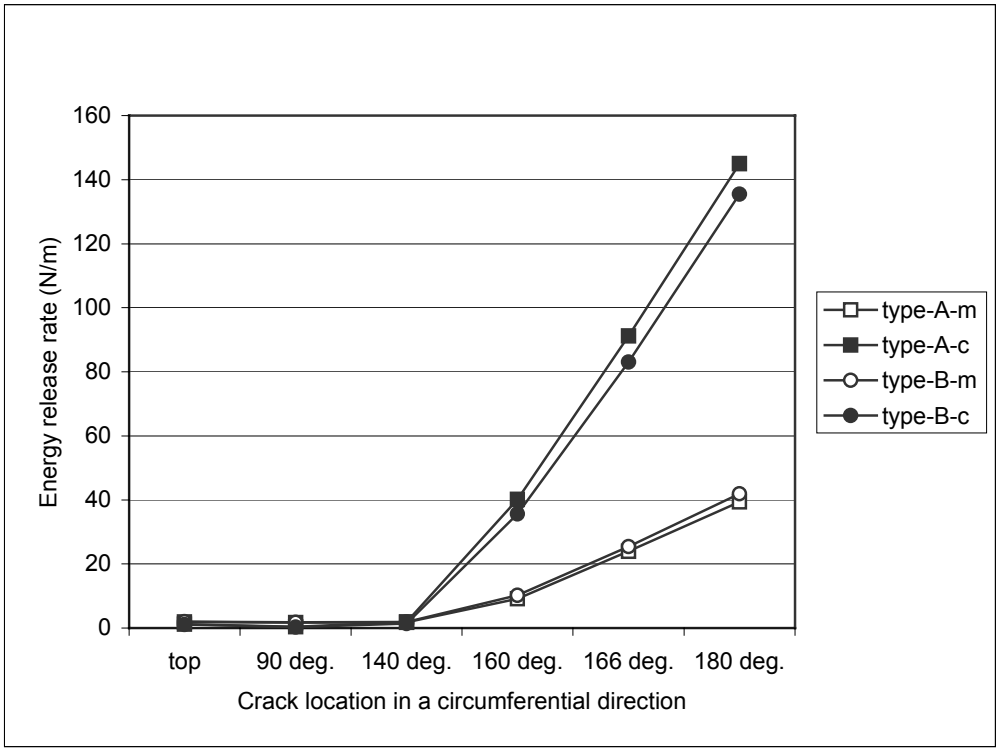

FIGURE 6.7 ─ J-integral with respect to different mesh density for static contact analysis of small crack (type-A: regular mesh, type-B: doubled mesh).

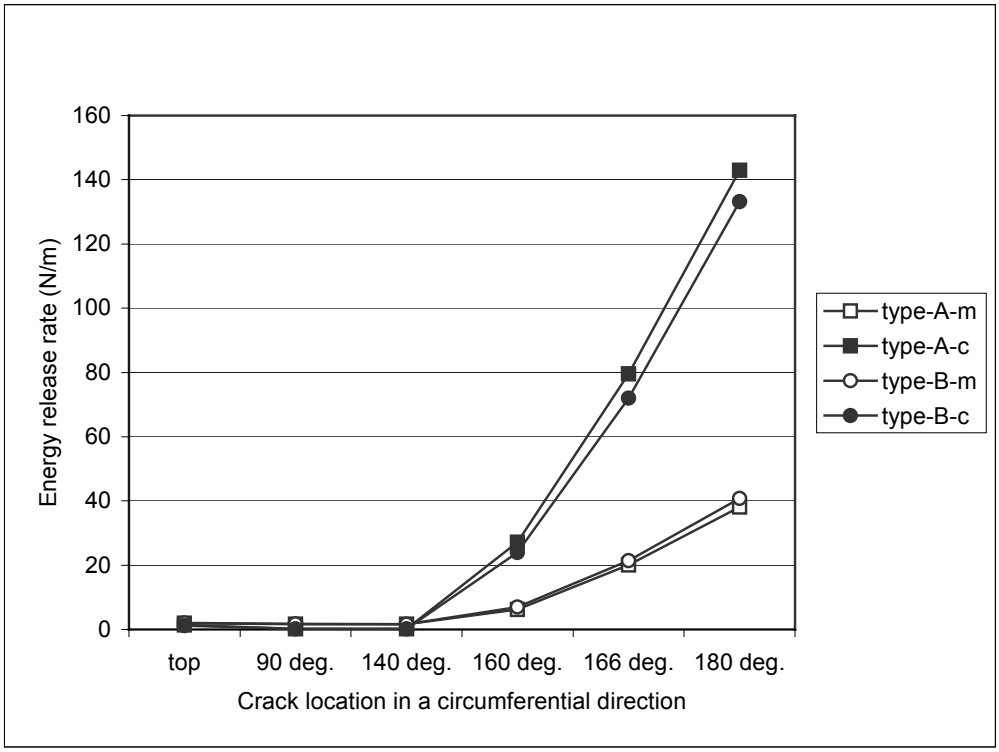

FIGURE 6.8 ─ J-integral with respect to different mesh density for traction analysis of small crack (type-A: regular mesh, type-B: doubled mesh).

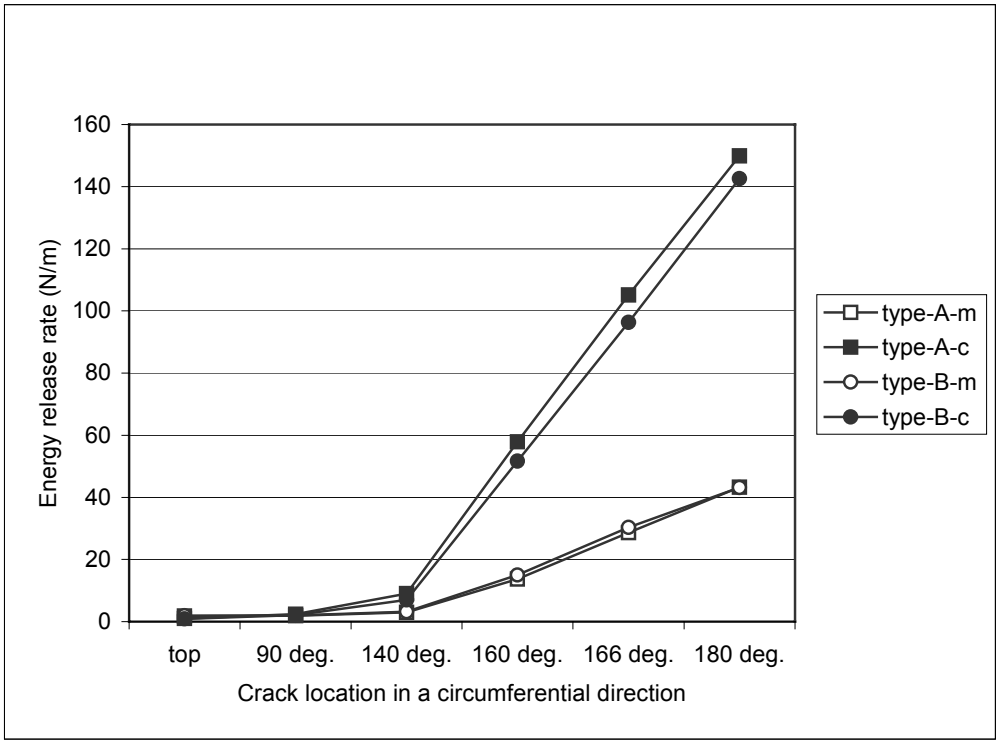

FIGURE 6.9 ─ J-integral with respect to different mesh density for braking analysis of small crack (type-A: regular mesh, type-B: doubled mesh).

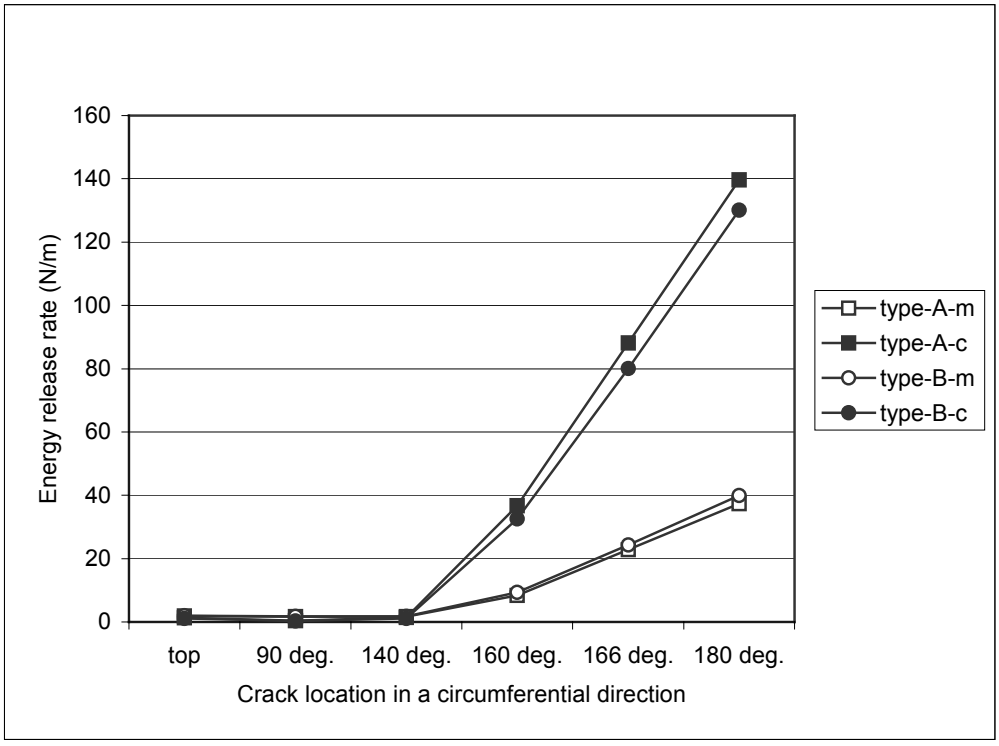

FIGURE 6.10 ─ J-integral with respect to different mesh density for free rolling analysis of small crack (type-A: regular mesh, type-B: doubled mesh).

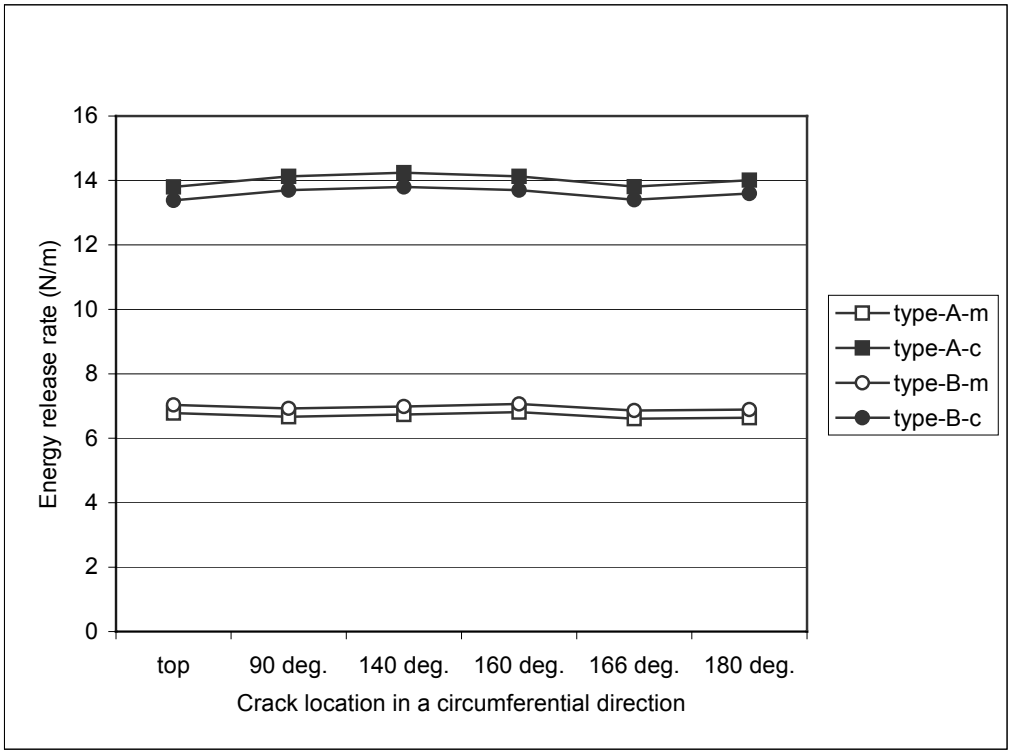

FIGURE 6.11 — J-integral with respect to different mesh density for inflation analysis of middle crack (type-A: regular mesh, type-B: doubled mesh).

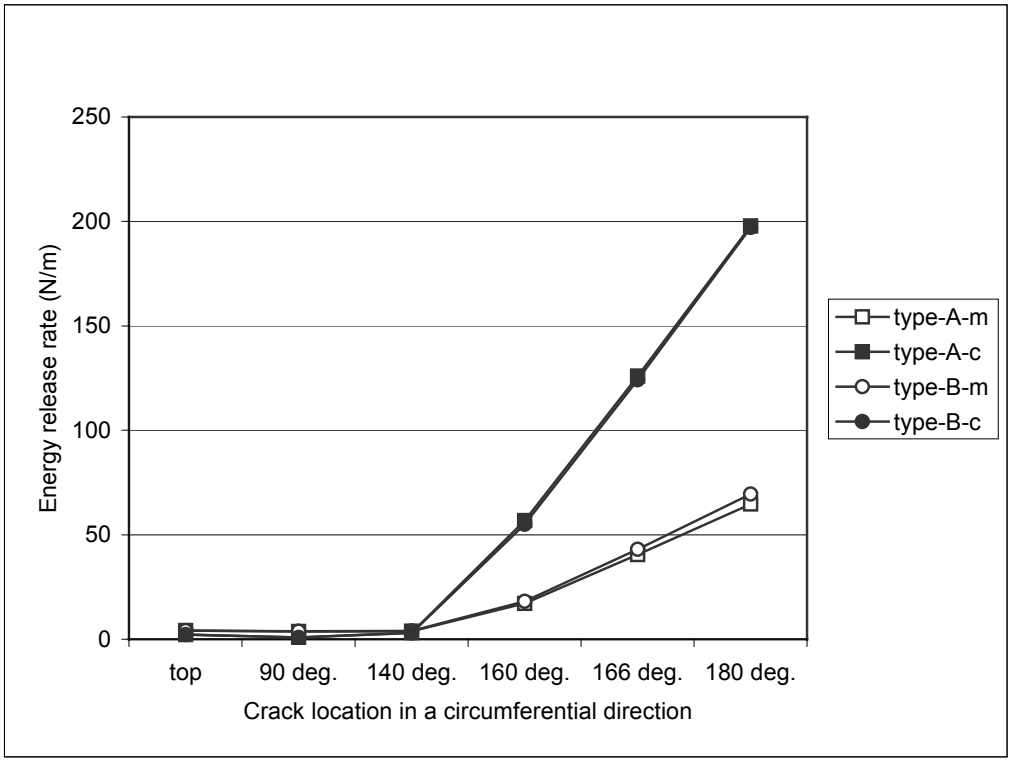

FIGURE 6.12 ─ J-integral with respect to different mesh density for static contact analysis of middle crack (type-A: regular mesh, type-B: doubled mesh).

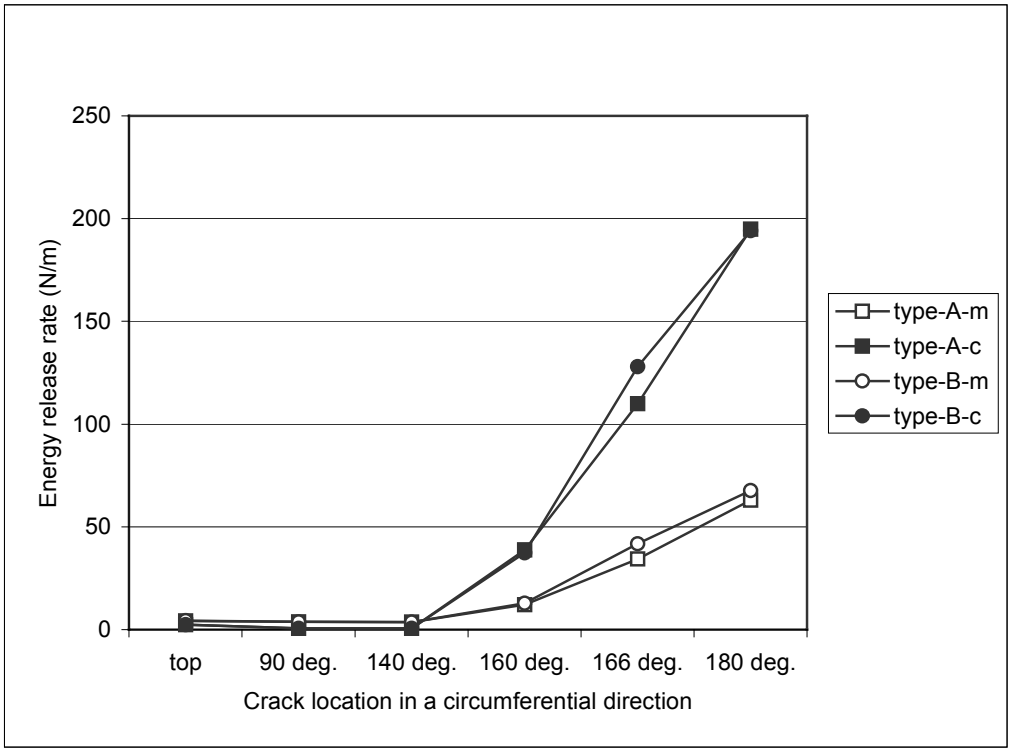

FIGRE 6.13 ─ J-integral with respect to different mesh density for traction analysis of middle crack (type-A: regular mesh, type-B: doubled mesh).

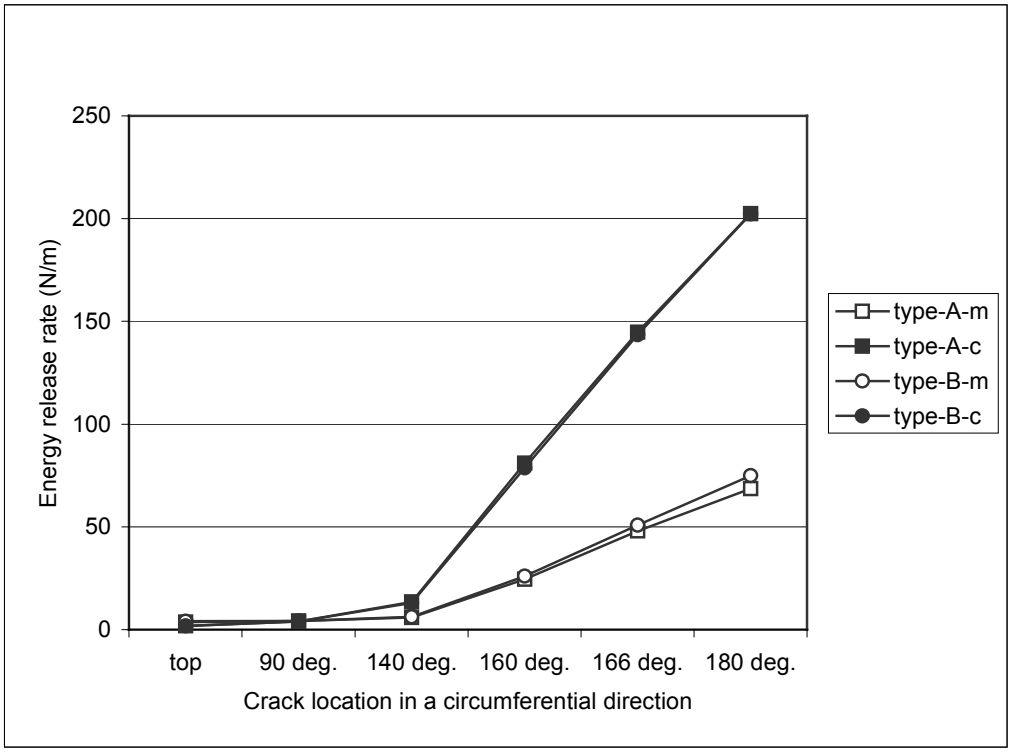

FIGURE 6.14 ─ J-integral with respect to different mesh density for braking analysis of middle crack (type-A: regular mesh, type-B: doubled mesh).

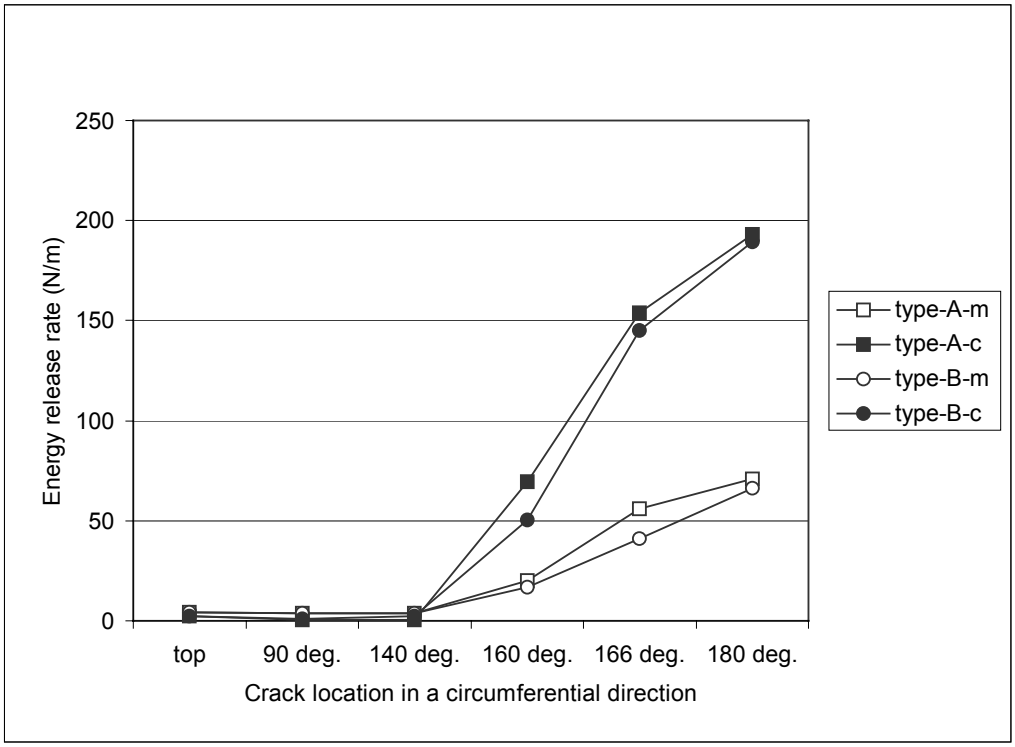

FIGURE 6.15 ─ J-integral with respect to different mesh density for free rolling analysis of middle crack (type-A: regular mesh, type-B: doubled mesh).

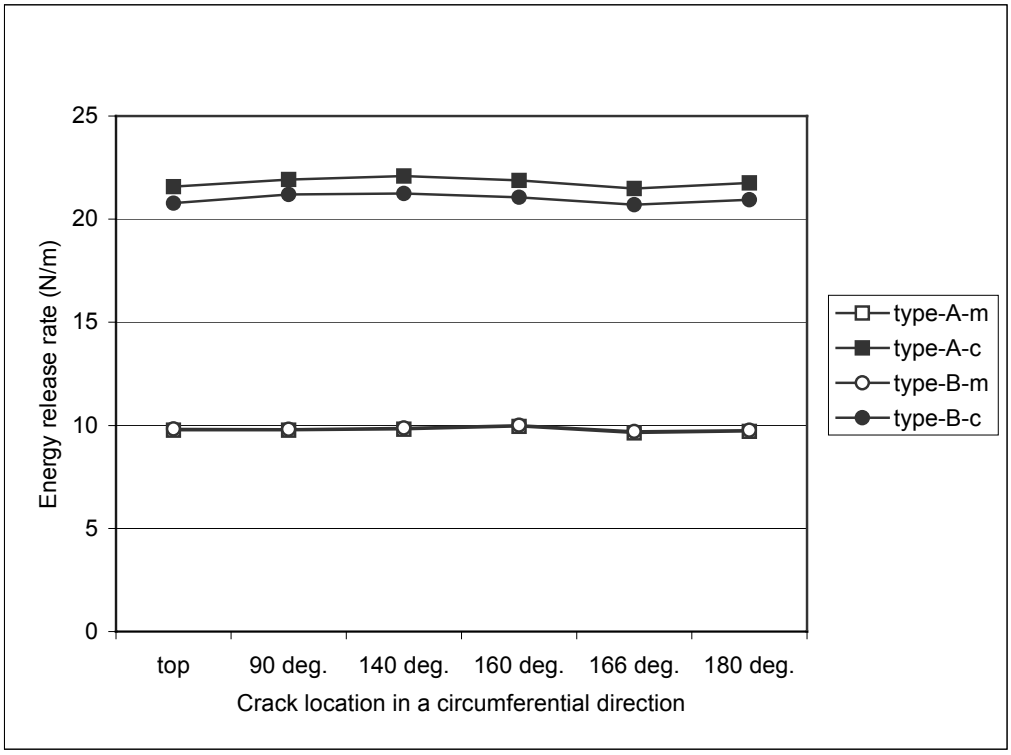

FIGURE 6.16 ─ J-integral with respect to different mesh density for inflation analysis of large crack (type-A: regular mesh, type-B: doubled mesh).

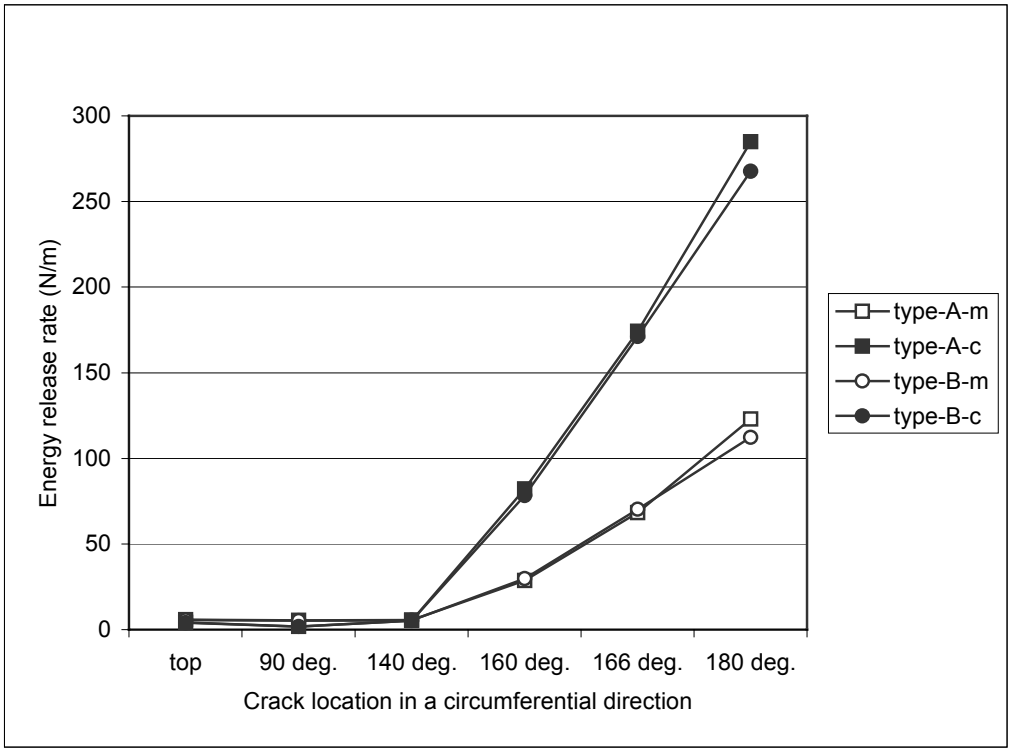

FIGURE 6.17 ─ J-integral with respect to different mesh density for static contact analysis of large crack (type-A: regular mesh, type-B: doubled mesh).

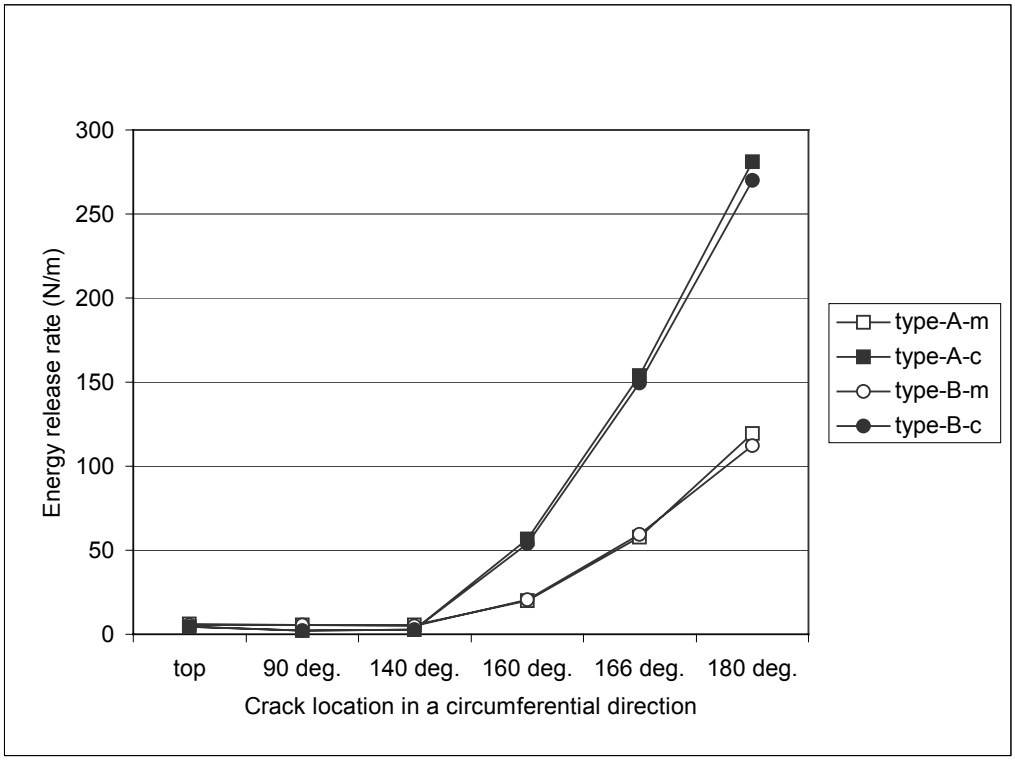

FIGURE 6.18 — J-integral with respect to different mesh density for traction analysis of large crack (type-A: regular mesh, type-B: doubled mesh).

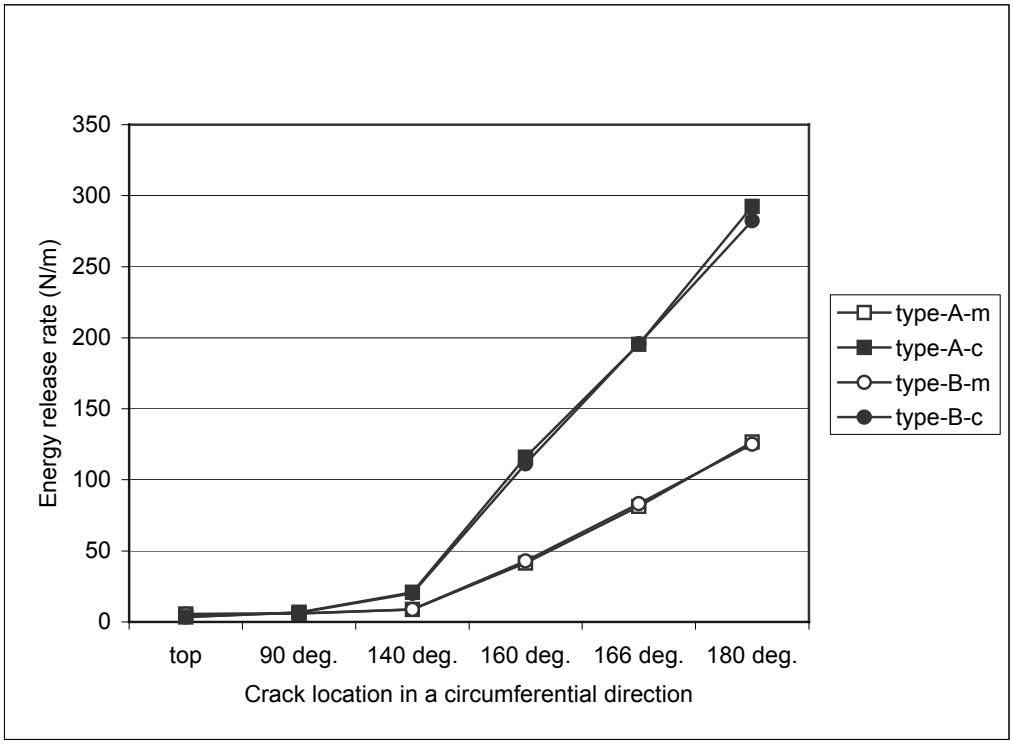

FIGURE 6.19 ─ J-integral with respect to different mesh density for braking analysis of large crack (type-A: regular mesh, type-B: doubled mesh).

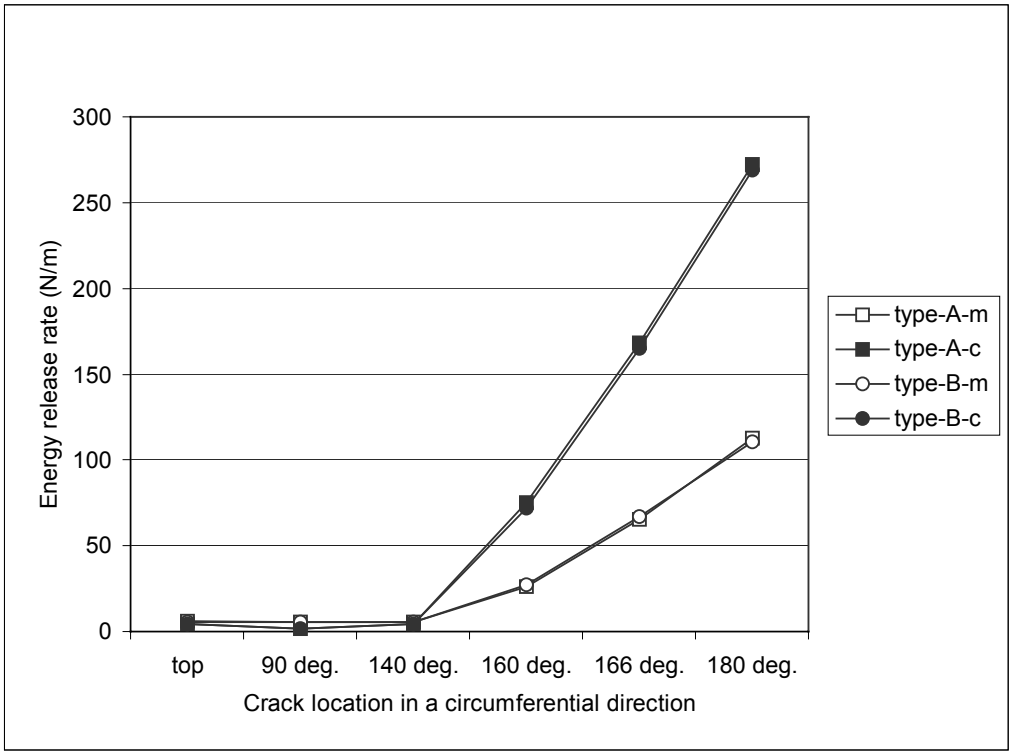

FIGURE 6.20 ─ J-integral with respect to different mesh density for free rolling analysis of large crack (type-A: regular mesh, type-B: doubled mesh).

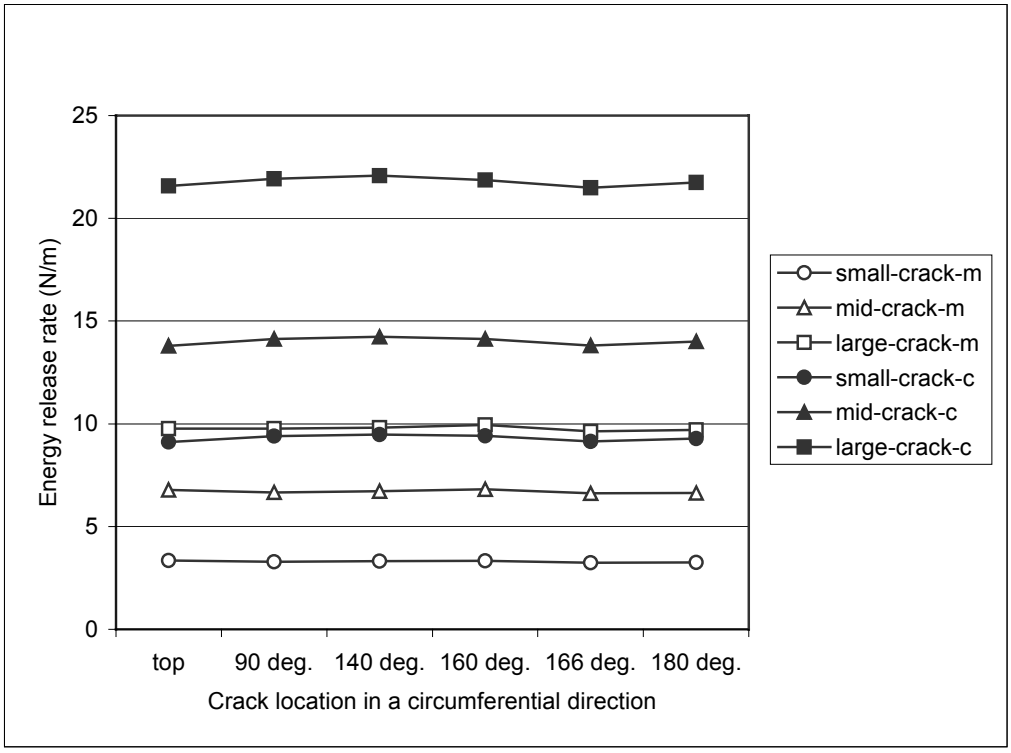

FIGURE 6.21 ─ J-integral with respect to different crack size for inflation analysis (regular mesh type).

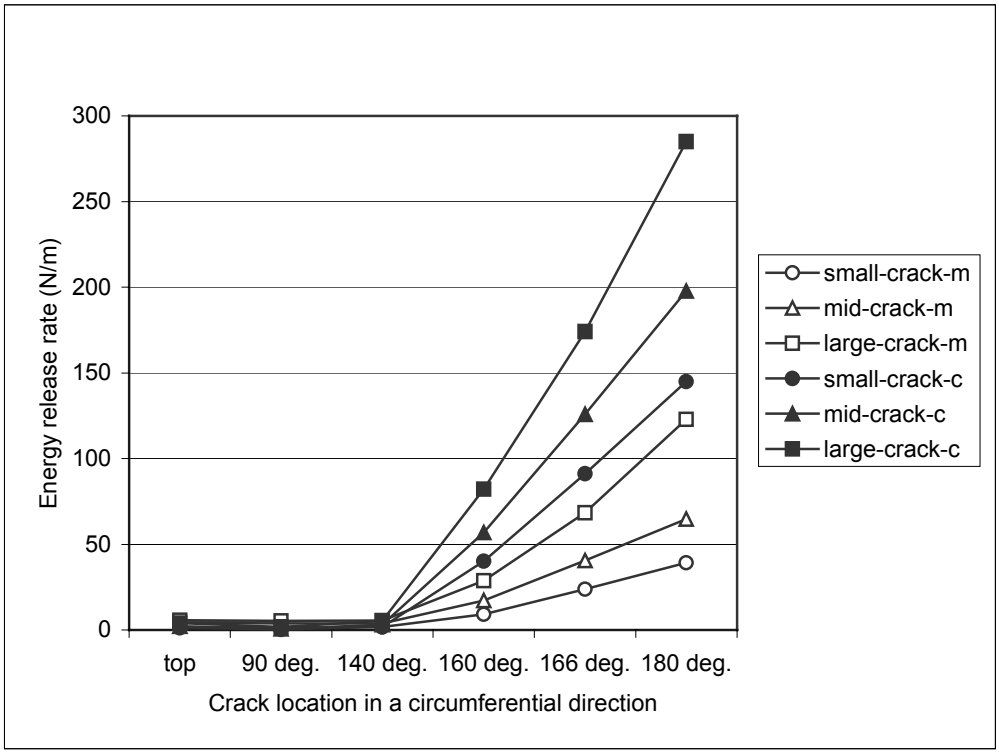

FIGURE 6.22 ─ J-integral with respect to different crack size for static contact analysis (regular mesh type).

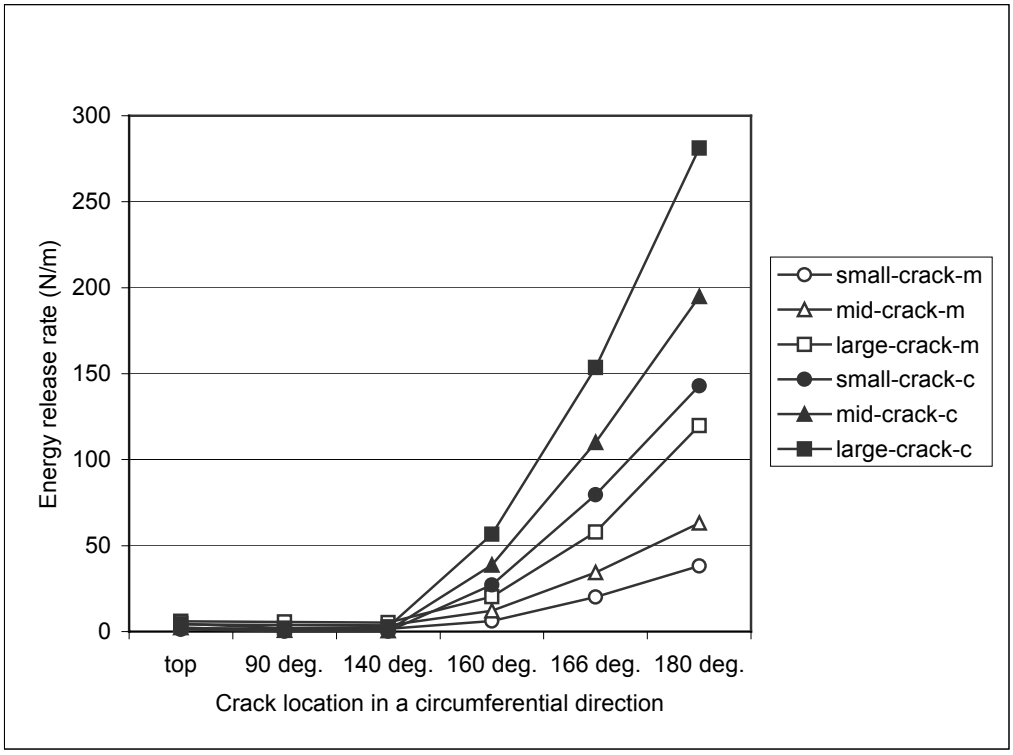

FIGURE 6.23 ─ J-integral with respect to different crack size for traction analysis (regular mesh type).

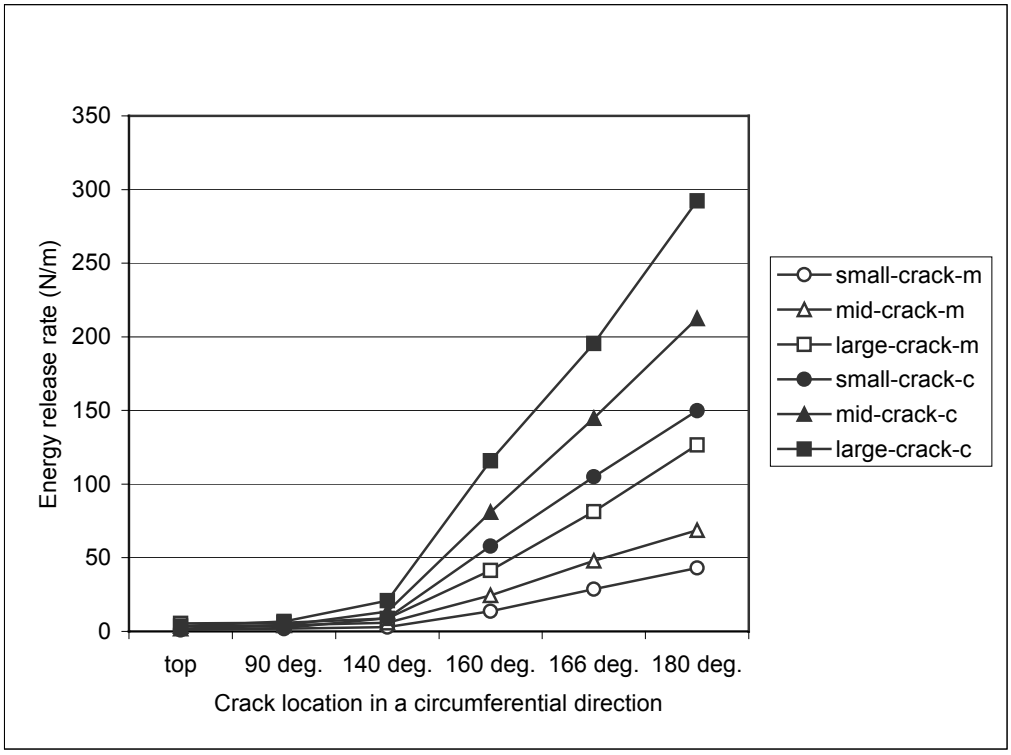

FIGURE 6.24 ─ J-integral with respect to different crack size for braking analysis (regular mesh type).

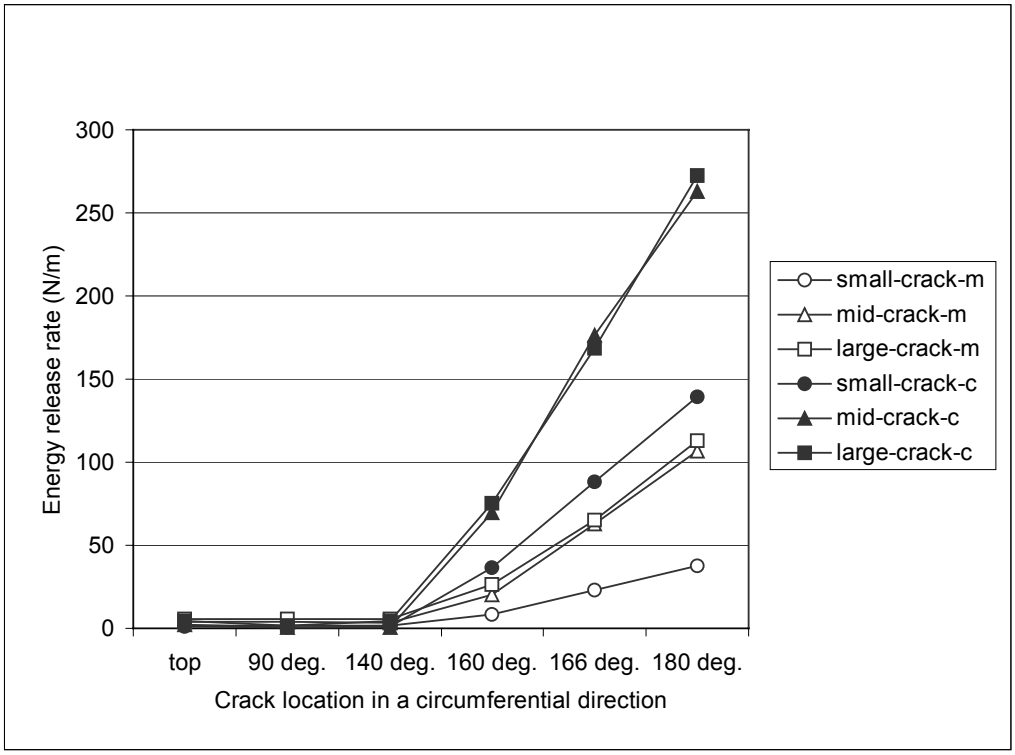

FIGURE 6.25 ─ J-integral with respect to different crack size for free rolling analysis (regular mesh type).

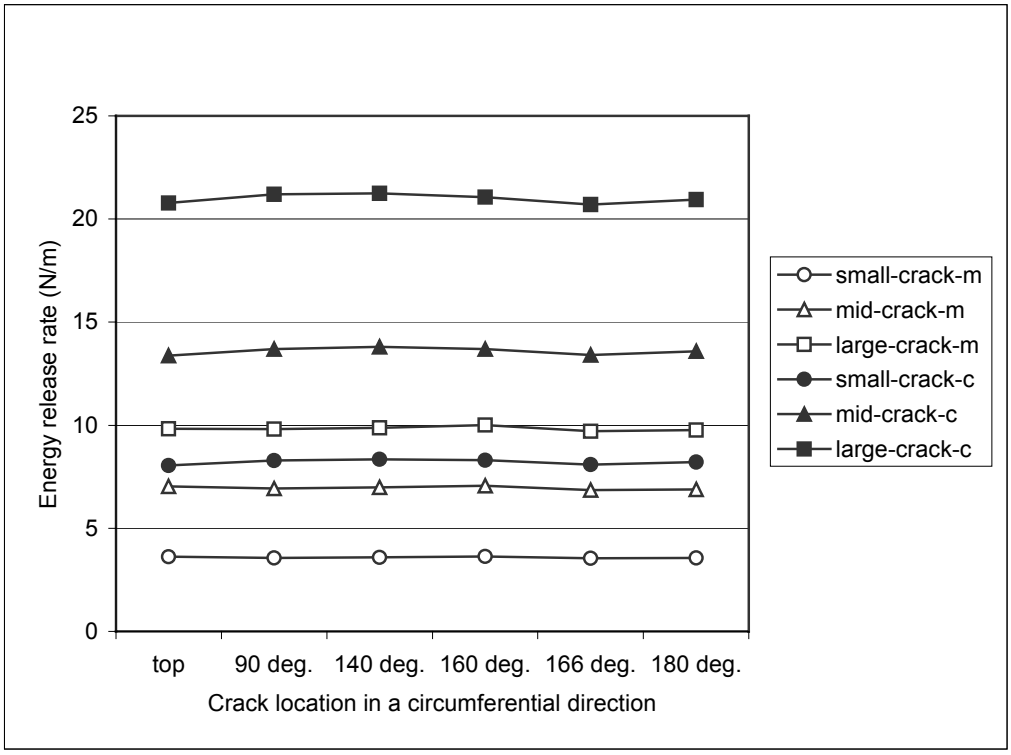

FIGURE 6.26 ─ J-integral with respect to different crack size for inflation analysis (doubled mesh type).

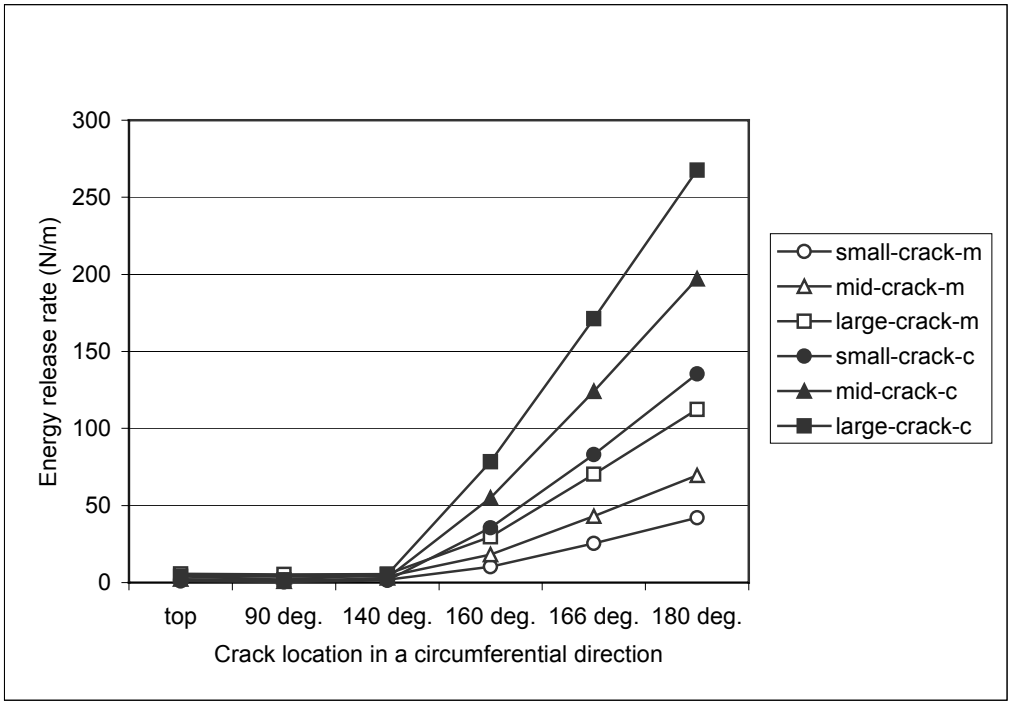

FIGURE 6.27 ─ J-integral with respect to different crack size for static contact analysis (doubled mesh type).

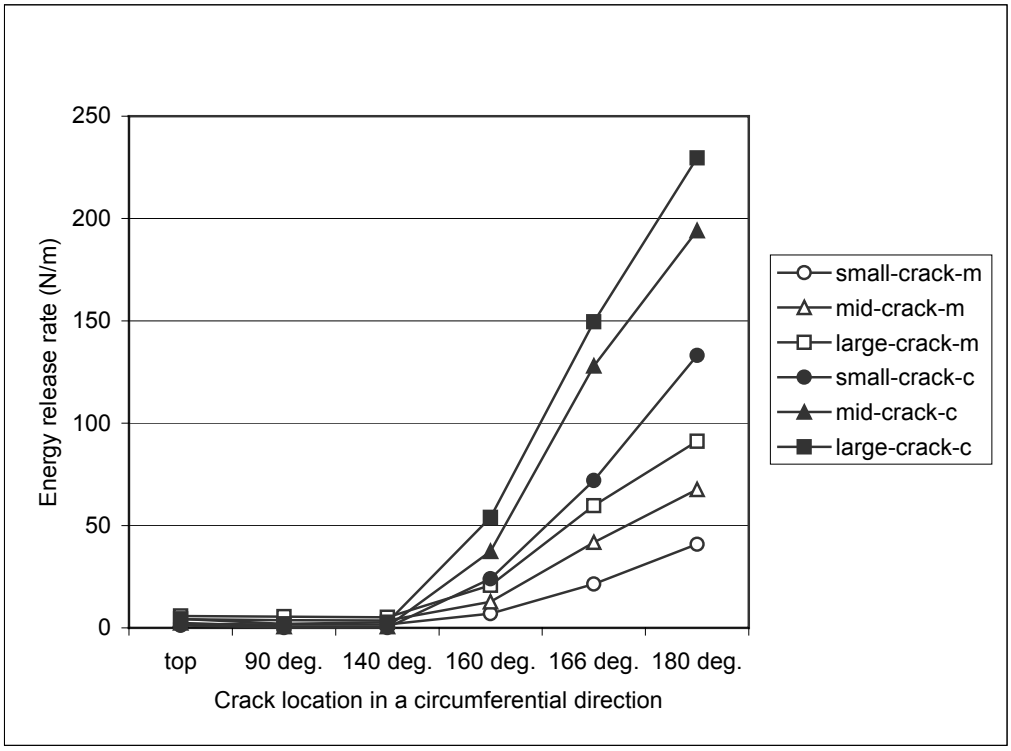

FIGURE 6.28 — J-integral with respect to different crack size for traction analysis (doubled mesh type).

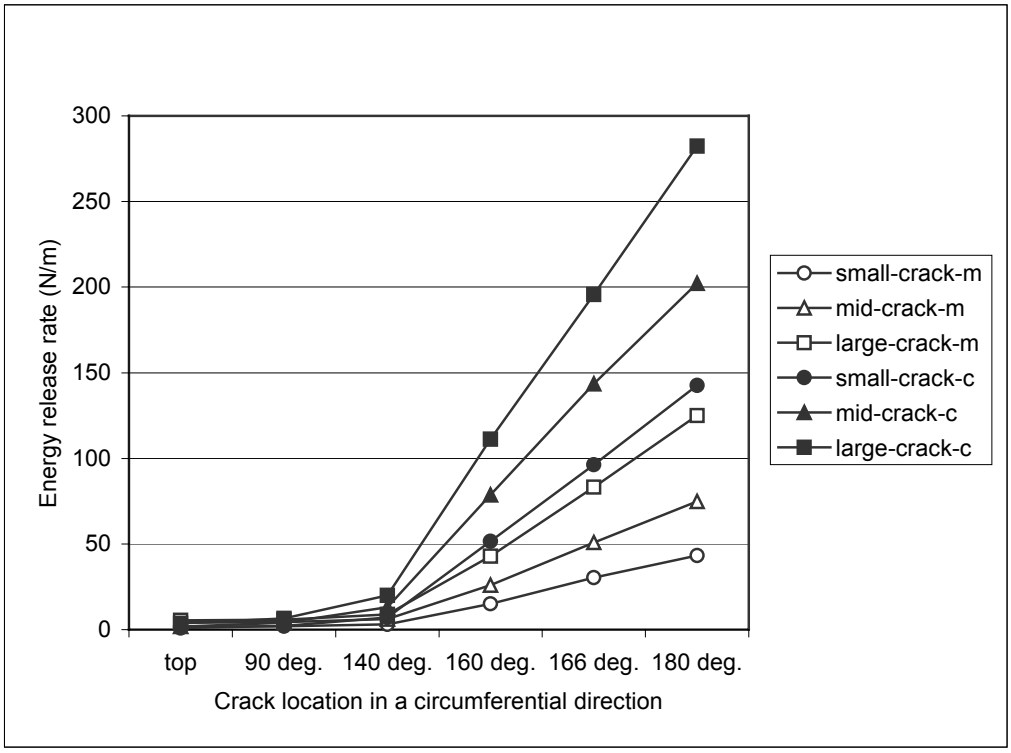

FIGURE 6.29 — J-integral with respect to different crack size for braking analysis (doubled mesh type).

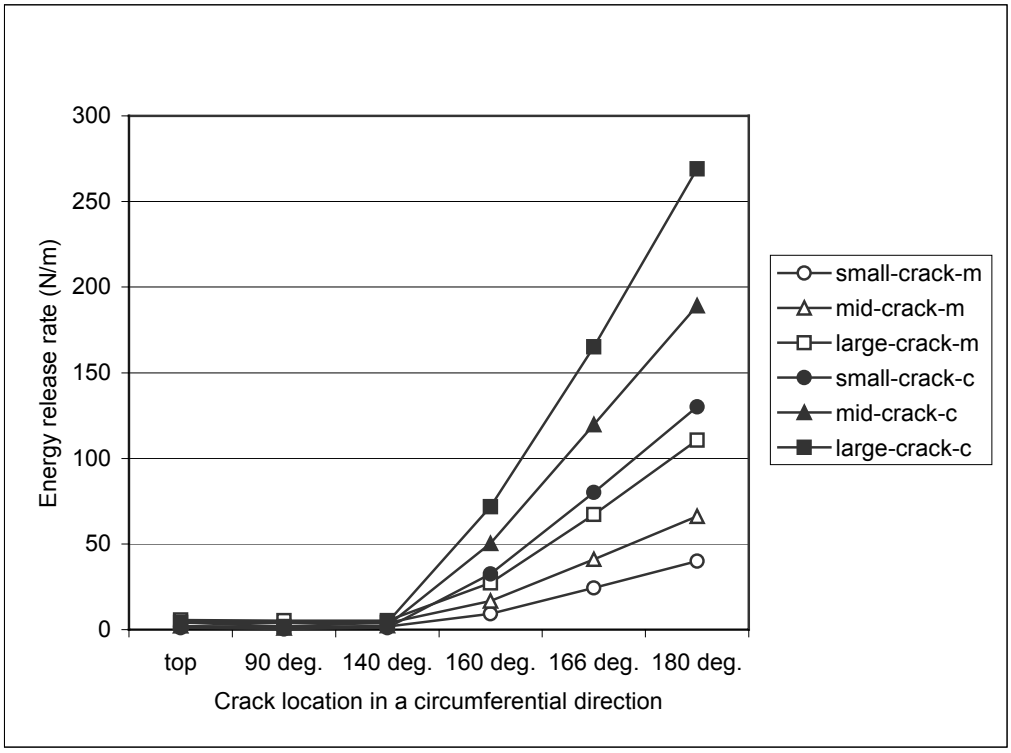

FIGURE 6.30 ─ J-integral with respect to different crack size for free rolling analysis (doubled mesh type).

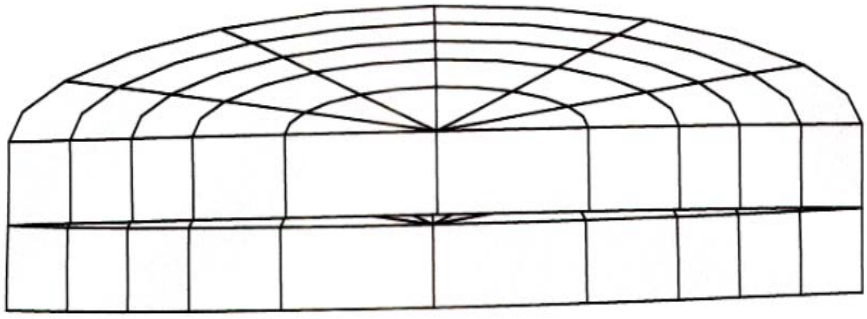

FIGURE. 6.31 ─ Crack mode shape for braking case, small crack and regular mesh type at the top region.

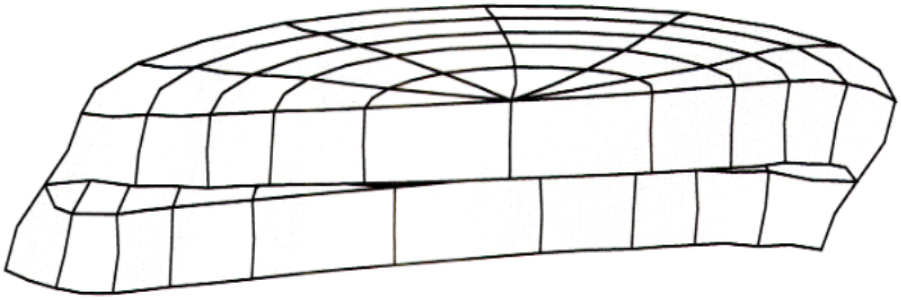

FIGURE. 6.32 ─ Crack mode shape for braking case, small crack and regular mesh type at the contact center region.

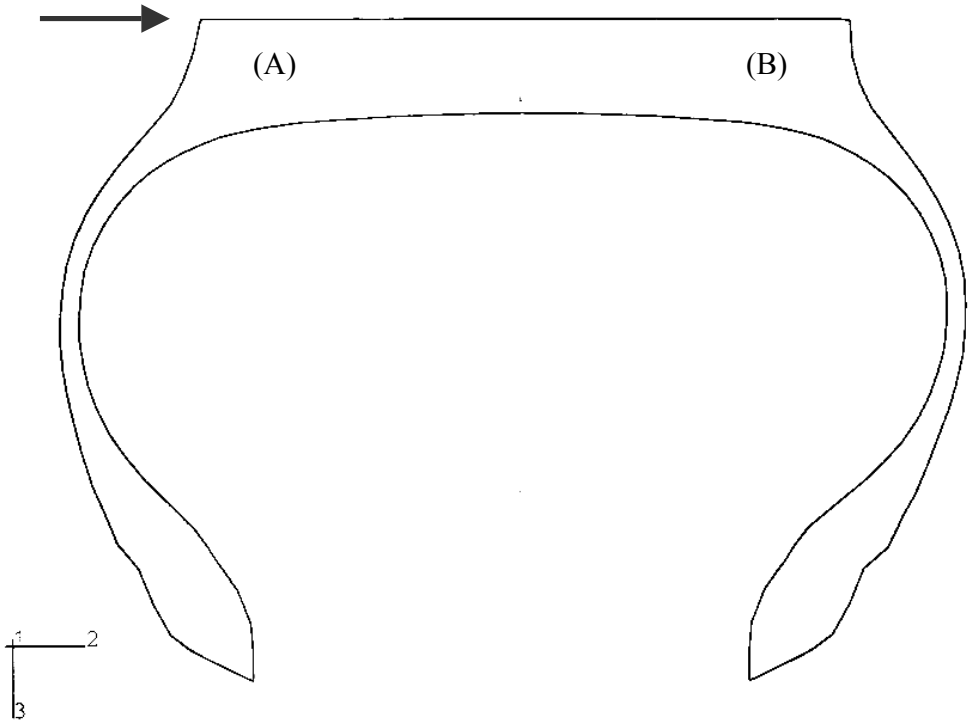

FIGURE 6.33 ─ Lateral loading boundary condition.

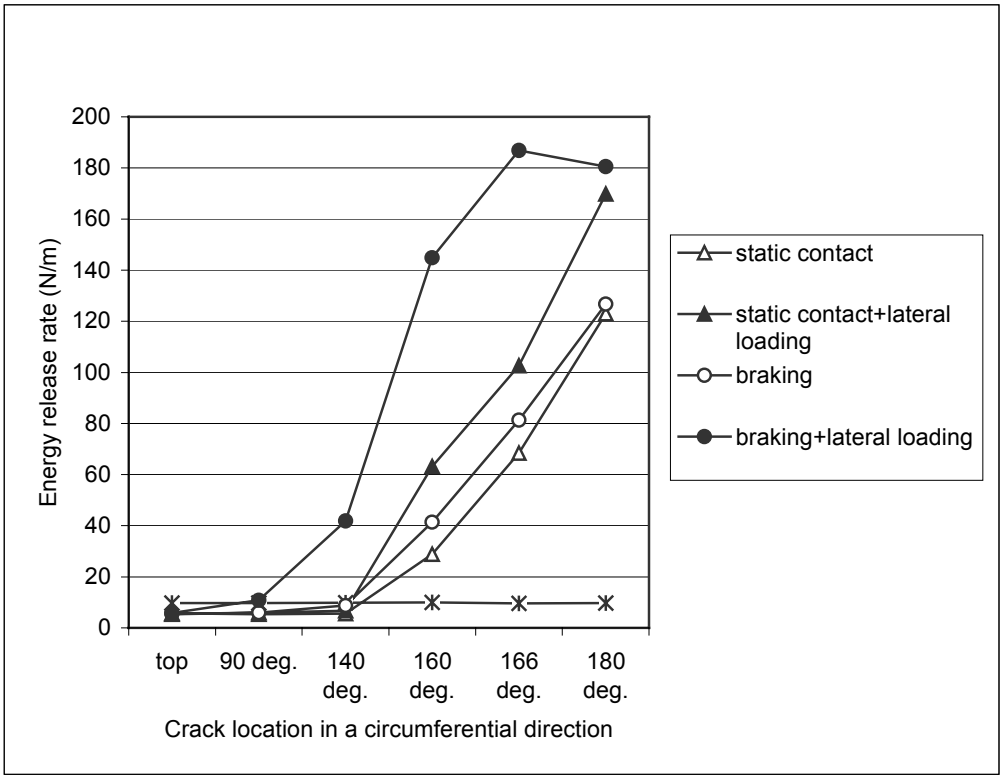

FIGURE 6.34 — J-integral with respect to different boundary conditions for large crack in a meridian direction (regular mesh type).

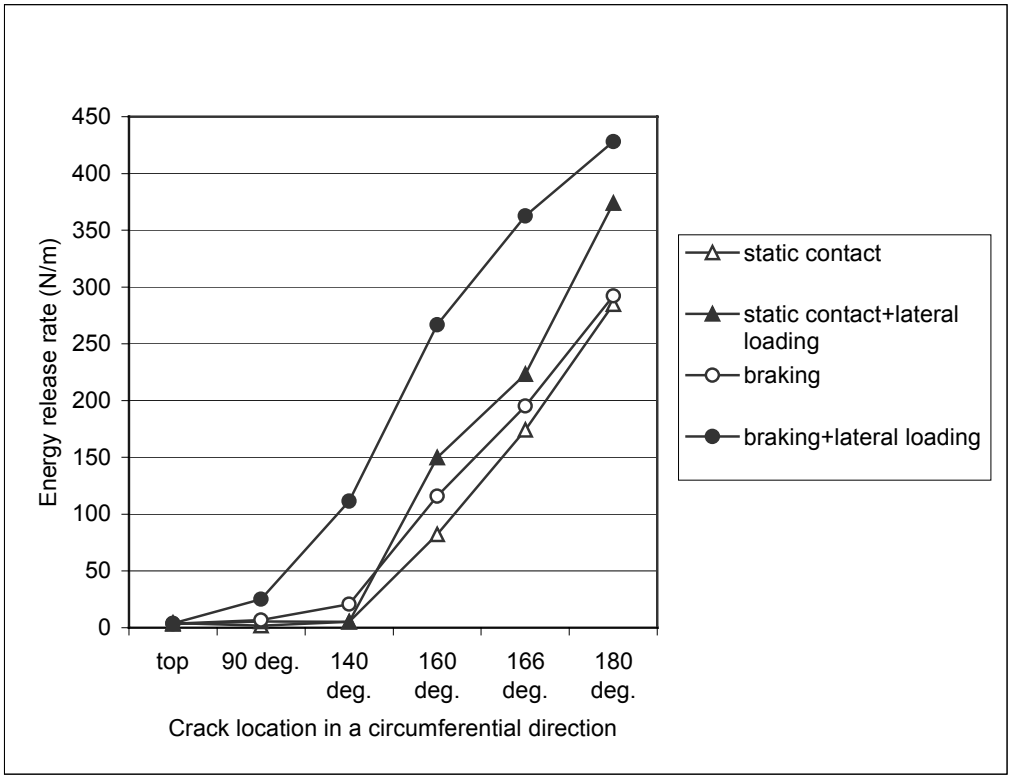

FIGURE 6.35 ─ J-integral with respect to different boundary conditions for large crack in a circumferential direction (regular mesh type).

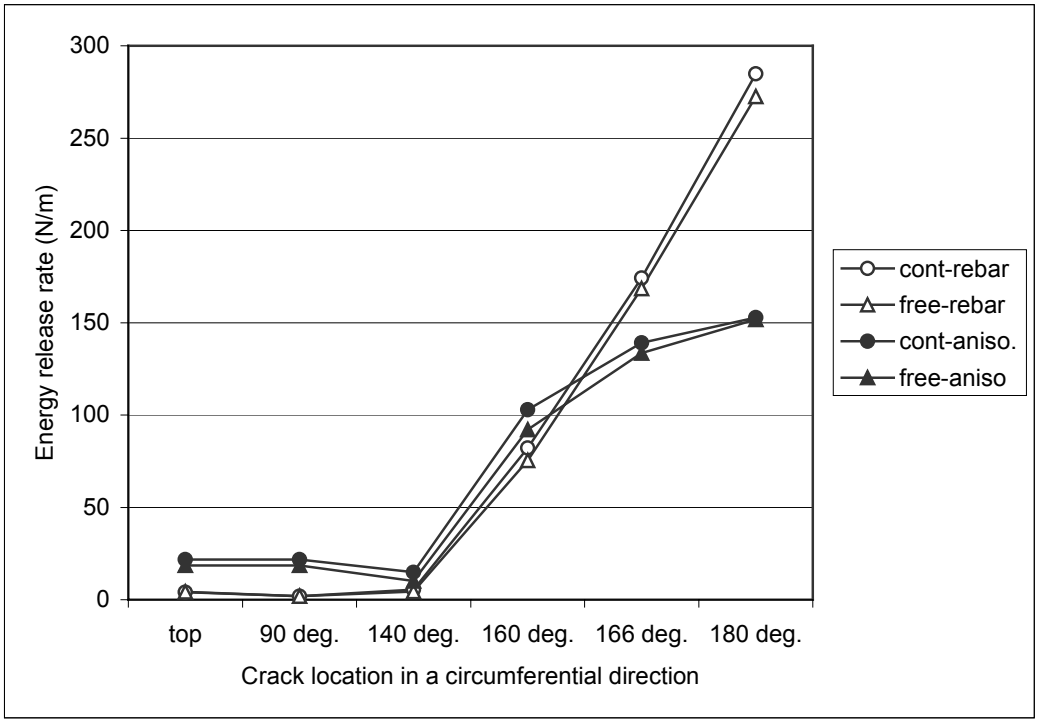

FIGURE 6.36 — Comparison of energy release rate: rebar vs. anisotropic for static contact and free rolling in a circumferential direction (regular mesh type, large crack).

TABLE 6.1 – Total number of elements in a local crack model.

	Regular-mesh type	Doubled-mesh type
Small-crack	780	1140
Mid-crack	900	1380
Large-crack	840	1200

CHAPTER VII

LIFETIME PREDICTION

The lifetime of a tire that is limited by belt separation can be approximately predicted by the energy release rates, as calculated in the previous Chapter. From equations (5.6) and (5.7), the total number of cycles can be expressed as:

$$N = \int_{length:ini-flaw}^{length:critical} \frac{dc}{A(\Delta G)^m} = \frac{1}{A(\Delta G)^m}[c_f - c_0] . \qquad (7.1)$$

A closed form of integral, equation (7.1), explains that lifetime depends on the crack size, material parameters and energy release rate. As shown in Table 5.1, ΔG varies by the crack size, and therefore, equation (7.1), for the total number of cycles, can be determined by summing the integrals representing each crack size. Thus the lifetime of a tire can be expressed by the number of cycle, N, which for three crack size intervals takes the form of:

$$N = \int_{c_0}^{c_1} \frac{dc}{A(\Delta G_1(c))^m} + \int_{c_1}^{c_2} \frac{dc}{A(\Delta G_2(c))^m} + \int_{c_2}^{c_f} \frac{dc}{A(\Delta G_3(c))^m} , \quad (7.2)$$

where $\Delta G_i(c)$ is an approximated linear function from Figure 7.1, which shows the trend the difference of energy release rate for free-rolling case of a regular type mesh. There is an alternative way to calculate the total number of cycles by using average values:

$$N = \sum_{k=1}^{n} (C_k - C_{k-1}) \frac{1}{A(\Delta G_k)^m}, \tag{7.3}$$

in which, n is the final crack size. The disadvantage of equation (7.3) is it doesn't consider an exact area under the curve therefore; closed form of integral equation (7.2) is used in this research. The material parameters used in the present study are introduced in reference [11]: $m=2.5;\ A=8.2e\text{-}8\ nm/(J/m^2)^{2.5}$. The values of energy release rate are listed in Table 5.1, with the different boundary conditions and different crack sizes for the regular-mesh type case. The total number of cycles, based on this approach, before belt separation is around 67,555,024 (215,846 ~ 229,429 km). The variation of total mileage results from the considering original radius of a tire and change of the amount of the vertical displacement (0.032m) when a tire is rolling. This result lies in the range of belt edge separation mileage, 137,000km~258,000km, in reference [12]. The variation of mileage with respect to an increase in crack size is represented in Figure 7.2.

We can figure out following important results from these two figures, Figure 7.1-7.2:

1. The propagation of the crack size is rather slow during the initial stage.
2. The propagation of the crack size increases dramatically with mileage to cause sudden failure.
3. The total mileage is highly correlated to an initial crack size

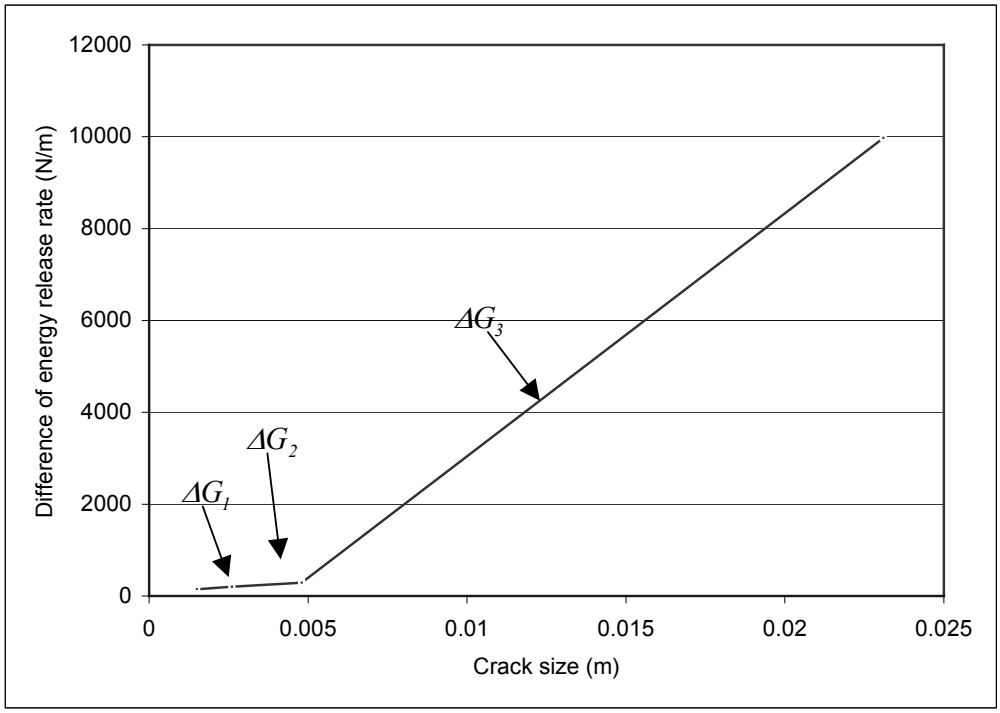

FIGURE 7.1 – Difference of G_{max} and G_{min} for free-rolling case of a regular type mesh.

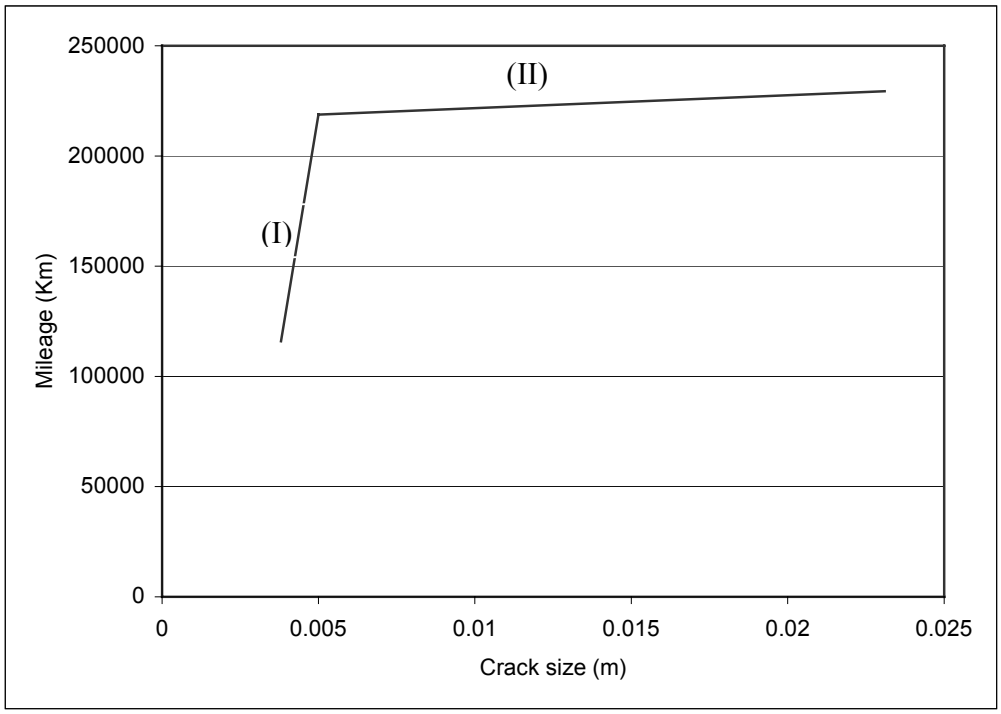

FIGURE 7.2 ─ Total mileages with respect to variation of crack.

CHAPTER VIII

CONCLUSION AND RECOMMENDATIONS

8.1 Summary

In this research a new cylindrical type of local finite element model has been suggested for predicting a tire lifetime. The suggested local model used a three-dimensional FEM fracture analysis, based on steady-state rolling assumption, in conjunction with a global-local technique. This study assumed that an initial flaw exists inside the tire, in the local model, due to a mechanical inhomogeneity introduced in the manufacturing of the tire. Within the local model, a J-integral variation study was performed in the crack region. Furthermore, it has been used to determine the crack growth rate analysis. The factors considered for comparison of energy release rate are: three different crack sizes; two different mesh densities; four different driving conditions; two different composite material calculation. The solutions are summarized as the following:

(1) Local symmetry crack model was suggested, based on the state of stress, in the belt edge rubber.

(2) In the inflation analysis, doubling the mesh near the crack front lines reduced the difference of the energy release rate in the circumferential and meridian directions.

(3) Higher values of energy release rate were obtained in a circumferential direction than in the meridian direction in any cases.

(4) Crack will propagate in the circumferential direction, followed by the meridian direction, from the comparison of energy release rate in both directions.

(5) Regardless of different crack sizes and driving conditions, energy release rate increased linearly at the location of 140^{o} from the top location.

(6) Opening mode is dominant at the top region, and mixed mode is dominant in the contact region.

(7) In the lateral loading case, combined with braking, higher values of energy release rate were obtained than any other driving conditions.

(8) In the anisotropic composite material application, the peak value of energy release rate at the contact center point is considerably smaller than the use of rebar element.

(9) The propagation of the crack size is rather slow during the initial stage.

(10) The propagation of the crack size increases dramatically with mileage to cause sudden failure.

(11) The total mileage is highly correlated to an initial crack size.

(12) The total mileage, obtained from this research, shows good correlation with reference data.

8.2 Recommendations for Further Research

Some topics about tire fracture mechanics analysis still open and deserve to be studied. Following summarized items are based on this research and author's research experience in tire (belt) durability.

(1) A study on the initial flaw size induced from manufacturing process.

The size of an initial flaw largely affects the total mileage, so it governs tire durability only if a tire does not contain an original damage in macroscopic sense. The initial flaw can be monitored and measured by a holographic technique or just from cut samples. It needs much iteration for choosing average value. Of course, better durability might be achieved in small initial flaw than large initial flaw. An initial flaw is related to the mechanical inhomogeneity during the curing of

tire in the mold. Therefore, the design of mold and rate of curing are important in minimizing the extent of flow orientation.

(2) A study on the different types of an initial flaw instigating crack.

It is very rare that a tire contains a circular type of an initial flaw, since mechanical inhomogeneity depends on the direction (circumferential and meridian direction). Therefore, analysis and comparison of energy release rate are needed for each different crack surface types.

(3) A study on the effect of thermal load.

Temperature rise in a rolling tire cause the degradation of material resilience and toughness, and leads to the reduction of fatigue endurance. A cyclic loading under service of a tire induces high heat build up inside the belt skims. The thermal expansions, in the heat build up area, are prohibited from taking transfer freely because of the restriction of free movement belt edge. This, together with nonuniform temperature profile due to mechanical anisotropy, induces thermal stress. For this, we have to know the temperature profile inside tire. Temperature profile, by finite element method, may be obtained the utilization of the generalized heat transfer equation. Reformulation of the stress-strain relationships, for linear elastic material, is needed to get the thermal stress.

(4) Unified test methods for evaluation the crack growth rate under mixed mode loading are needed.

Appendix

This appendix explains the relation of local and global coordinate system. It may be used for material transformation and local outputs when we need it. Specifically in tire problems, local outputs such as stress, strain and displacement are important due to the effect of tire geometry and material complexity. The relation of local and global coordinate system is defined by the transformation matrix [T], and it is represented in the following user subroutine for the given element numbering.

```
     *USER SUBROUTINE
      SUBROUTINE ORIENT(T,NOEL,NPT,LAYER,KSPT,COORDS,BASIS,
     1 ORNAME,NNODES,CNODES,JNNUM)
C
      INCLUDE 'ABA_PARAM.INC'
C
      CHARACTER*80 ORNAME
C
C
C
C
C
C
C
C
C
C
C
      DIMENSION T(3,3),COORDS(3),BASIS(3,3),CNODES(3,NNODES)
      DIMENSION JNNUM(NNODES)

C
C     PLANE 1-4-8-5
C
      XM1=(CNODES(1,1)+CNODES(1,4)+CNODES(1,8)+CNODES(1,5))/4.D0
```

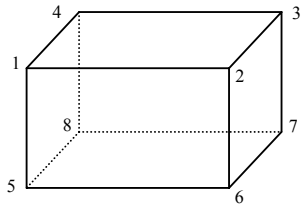

```
      YM1=(CNODES(2,1)+CNODES(2,4)+CNODES(2,8)+CNODES(2,5))/4.D0
      ZM1=(CNODES(3,1)+CNODES(3,4)+CNODES(3,8)+CNODES(3,5))/4.D0
C
C     PLANE 2-3-7-6
C
      XM2=(CNODES(1,2)+CNODES(1,3)+CNODES(1,7)+CNODES(1,6))/4.D0
      YM2=(CNODES(2,2)+CNODES(2,3)+CNODES(2,7)+CNODES(2,6))/4.D0
      ZM2=(CNODES(3,2)+CNODES(3,3)+CNODES(3,7)+CNODES(3,6))/4.D0
C
C     PLANE 5-6-7-8
C
      XC1=(CNODES(1,5)+CNODES(1,6)+CNODES(1,7)+CNODES(1,8))/4.D0
      YC1=(CNODES(2,5)+CNODES(2,6)+CNODES(2,7)+CNODES(2,8))/4.D0
      ZC1=(CNODES(3,5)+CNODES(3,6)+CNODES(3,7)+CNODES(3,8))/4.D0
C
C     PLANE 1-2-3-4
C
      XC2=(CNODES(1,1)+CNODES(1,2)+CNODES(1,3)+CNODES(1,4))/4.D0
      YC2=(CNODES(2,1)+CNODES(2,2)+CNODES(2,3)+CNODES(2,4))/4.D0
      ZC2=(CNODES(3,1)+CNODES(3,2)+CNODES(3,3)+CNODES(3,4))/4.D0
C
C     PLANE 1-5-6-2
C
      XV1=(CNODES(1,1)+CNODES(1,5)+CNODES(1,6)+CNODES(1,2))/4.D0
      YV1=(CNODES(2,1)+CNODES(2,5)+CNODES(2,6)+CNODES(2,2))/4.D0
      ZV1=(CNODES(3,1)+CNODES(3,5)+CNODES(3,6)+CNODES(3,2))/4.D0
C
C     PLANE 8-7-3-4
C
      XV2=(CNODES(1,8)+CNODES(1,7)+CNODES(1,3)+CNODES(1,4))/4.D0
      YV2=(CNODES(2,8)+CNODES(2,7)+CNODES(2,3)+CNODES(2,4))/4.D0
      ZV2=(CNODES(3,8)+CNODES(3,7)+CNODES(3,3)+CNODES(3,4))/4.D0
C
      DMX=XM2-XM1
      DMY=YM2-YM1
      DMZ=ZM2-ZM1
      DCX=XC2-XC1
      DCY=YC2-YC1
      DCZ=ZC2-ZC1
      DVX=XV2-XV1
```

```
      DVY=YV2-YV1
      DVZ=ZV2-ZV1
C
      DLM=DSQRT(DMX*DMX+DMY*DMY+DMZ*DMZ)
      DLC=DSQRT(DCX*DCX+DCY*DCY+DCZ*DCZ)
      DLV=DSQRT(DVX*DVX+DVY*DVY+DVZ*DVZ)
C
C     DIRECTION COSINE
C
      DO 500 I=1,3
      DO 500 J=1,3
500   T(I,J)=0.0
      T(1,1)=DMX/DLM
      T(2,1)=DMY/DLM
      T(3,1)=DMZ/DLM
      T(1,2)=DCX/DLC
      T(2,2)=DCY/DLC
      T(3,2)=DCZ/DLC
      T(1,3)=DVX/DLV
      T(2,3)=DVY/DLV
      T(3,3)=DVZ/DLV
C     WRITE(6,200) NOEL,NPT,ALPH,T(1,1),T(2,1),T(3,1),T(1,2),T(2,2),
C
100   FORMAT(A10)
200   FORMAT(2I5,F9.2,9F7.2)
      RETURN
      END
```

References

[1] A. Stevenson, *A fracture mechanics study of the fatigue of rubber in compression*, Int. Journal of Fracture, Vol. 23, 1983, pp. 47-59.

[2] D. C. Prevorsek, C. W. Beringer, I. Rally and Y. D. Kwon, *Application of Fracture Mechanics in Tire Endurance Analysis*, Tire Society Meeting, 1984.

[3] D. G. Young, *Application of Fatigue Methods Based on Fracture Mechanics for Tire Compound Development*, Rubber Chemistry and Technology, Vol. 63, 1990.

[4] J. H. Chang and E. B. Becker, *Finite Element Calculation of Energy Release Rate for 2-D Rubbery Material Problems with Non-Conservative Crack Surface Tractions*, International Journal for Numerical Methods in Engineering, Vol. 33, 1992, pp. 907-927.

[5] R. M. V. Pidaparti, Henry T. Y. Yang, W. Soedel, *Modeling and Fracture Prediction of Single Cord-Rubber Composites*, Journal of Composite Materials, Vol. 26, No. 2, 1992.

[6] G. J. Lake, *Fatigue and fracture of elastomers*, Rubber Chemistry and Technology, Vol. 68, 1995, pp. 435-460.

[7] T. G. Ebbott, *An Application of Finite Element-Based Fracture Mechanics Analysis to Cord-Rubber Structures*, Tire Science and Technology, Vol. 24, No. 3

, 1996, pp. 220-235.

[8] Masaharu Iwamoto, Qing-Qing Ni, Teruhiko Fujiwara, and Ken Kurashiki, *Interlaminar fracture mechanism in unidirectional CFRP composites part II: analysis*, Engineering Fracture Mechanics, Vol. 64, Issue 6, 1999.

[9] T. G. Ebbott, R. L. Hohman, J. P. Jeusette, and V. Kerchman, *Tire Temperature and Rolling Resistance Prediction with Finite Element Analysis*, Tire Science and Technology, Vol. 22, No. 1, 1999, pp. 2-21.

[10] Wei, Y-T., Tian, and Du, X. W., *A Finite Element Model for the Rolling Loss Prediction and Fracture Analysis of Radial Tires*, Tire Science and Technology, Vol. 27, No. 4, 1999, pp. 250-276.

[11] S. Govindjee, *Firestone Tire Failure Analysis*, (http://www.ce.berkeley.edu/~sanjay/), 2001.

[12] S. E. Gelosa, G. Ratti and H. Moneypenny, *Design Truck Tyres with Safety and Durability*, BRITE/EURAM Project RI 1B-274, 1993.

[13] G. P. Giuliani, G. Medri, and A. Pirondi, *A Test to Evaluate Fatigue Crack Growth in Rubber Compounds under Mixed Mode Loading*, Tire Science and Technology, Vol. 29, No. 1, 2001, pp. 44-55.

[14] J. R. Rice, *Mathematical analysis in the mechanics of fracture*, 1968, pp. 191-213.

[15] R. S. Rivilin and A. G. Thomas, *Rupture of rubber, I. Characteristics energy for tearing*, Polymer Science and Technology, 1953, pp. 291-318.

[16] O. Allix, P. Ladeveze, *Damage analysis of interlaminar fracture specimens*, Composite Structures, Vol. 31, 1995, pp. 61-74.

[17] Alberto Corigliano, *Formulation, Identification and Use of Interface Models in the Numerical Analysis of Composite Delamination*, Journal of Solid Structures, Vol. 30, No. 20, 1993, pp. 2779-2811.

[18] B. D. Davidson and R. A. Schapery, *A Technique for Predicting Mode I Energy Release Rates Using a First-Order Shear Deformable Plate Theory*, Engineering Fracture Mechanics, Vol. 36, No. 1, pp. 157-165, 1990.

[19] Renato Barboni, Rolando Carbonaro and Paolo Gaudenzi, *The Effects of Delamination on the Fatigue Behavior of Composite Structures*, Journal of Composite Materials, Vol. 33, No. 3, 1999.

[20] D. J. Lee and J. A. Donovan, *Mixed mode I and II fracture of carbon black filled natural rubber*, International Journal of Fracture, Vol. 34, 1987, pp. 41-55.

[21] Y. Mi, M. A. Crisfield, and G. A. O. Davies, *Progressive Delamination Using Interface Elements*, Journal of Composite Materials, Vol. 32, No. 14, 1998.

[22] James R. Reeder and John H. Crews Jr., *Mixed-Mode Bending Method for Delamination Testing*, AIAA Journal, Vol. 28, No. 7, 1990.

[23] K. Grosch, *Rolling Resistance and Fatigue Life of Tires*, Rubber Chemistry and Technology, Vol. 61, 1988.

[24] E. F. Rybicki and M. F. Kanninen, *A Finite Element Calculation of Stress Intensity Factors by a Modified Crack Closure Integral*, Engineering Fracture Mechanics, Vol. 9, 1977, pp. 931-938.

[25] Gerhard A. Holzapfel, Thomas C. Gasser, *A viscoelastic model for fiber-reinforced composites at finite strains: Continuum basis, computational aspects and applications*, Computer methods in applied mechanics and engineering, Vol. 190, 2001, pp. 4379-4403.

[26] S. Mark Spearing and Peter W. R. Beaumont, *Towards a Predictive Design Methodology Based on the Physical Modelling of the Fracture of Fiber Composites*, Applied Composite Materials, Vol. 5, 1998, pp. 69-94.

[27] Alberto Corigliano and Olivier Allix, *Some aspects of interlaminar degradation in composites*, Computer methods in applied mechanics and engineering, Vol. 185, 2000, pp. 203-224.

[28] W. V. Mars, *Multiaxial Fatigue of Rubber*, PhD Dissertation, 2001.

[29] Y. Liu, Z. Wan, X. Du, J. Jiang, and M. Yao, *Fatigue of Unidirectional Cord-Rubber Composites*, Tire Science and Technology, Vol. 27, No. 1, 1999, pp. 48-57.

[30] D. Dalmas and A. Laksimi, *On the Method of Determination of Strain Energy Release Rate During Fatigue Delamination in Composite Materials*, Applied Composite Materials, Vol. 6, 1999, pp. 327-340.

[31] Pappu L. N. Murthy and Christos C. Chamis, *Composite Interlaminar Fracture Toughness: Three-Dimensional Finite-Element Modeling for Mixed Mode I, II, and Fracture*, Composite Materials, 1988, pp. 23-40.

[32] R. M. V. Pidaparti and A. W. May, *Stress Analysis of Failures in Cord-Rubber Composites*, Polymers & Polymer Composites, Vol. 9, No. 1, 2001.

[33] Joseph D. Walter, *Cord-Rubber Tire Composites: Theory and Applications*, Rubber Chemistry and Technology, Vol. 51, pp. 525-576.

[34] Farhad Tabaddor, *Mechanical Properties of Cord-Rubber Composites, Composite Structures*, Vol. 3, 1985, pp. 33-53.

[35] Hui-Zu Shan & Tsu-Wei Chou, *Transverse Elastic Moduli of Unidirectional Fiber Composites with Fiber/Matrix Interfacial Debonding*, Composites Science and Technology, Vol. 53, 1995, pp. 383-391.

[36] Ruey-Bin Yang and Ajit K. Mal, *The Effective Transverse Moduli of A Composite with Degraded Fiber-Matrix Interfaces*, Int. J. Engineering Science, Vol. 33, No. 11, 1995, pp. 1623-1632.

[37] R. M. V. Pidaparti & A. W. May, *A micromechanical analysis to predict the cord-rubber composites properties*, Composite Structures, Vol. 34, 1996, pp. 361-369.

[38] Y. Liu, Z. Wan, X. Du, J. Jiang, and M. Yao, *Fatigue of Unidorectional Cord-Rubber Composites*, Tire Science and Technology, Vol. 27, 1999, pp. 48-57.

[39] Alfredo Balaco de Morais, *Transverse moduli of continuous-fibre-reinforced polymers*, Composites Science and Technology, Vol. 60, 2000, pp. 997-1002.

[40] G. Duvaut, G. Terrel, F. Lene, V. E. Verijenko, *Optimization of fiber reinforced composites, Composite Structures*, Vol. 48, 2000, pp. 83-89.

[41] W. W. Curtiss, *Principles of Tire Design*, Tire Science and Technology, Vol. 1, No. 1, 1973, pp. 77-98.

[42] R. B. Day and S. D. Gehman, *Theory for the Meridian Section of Inflated Cord Tires*, Rubber Chemistry and Technology.

[43] O. B. Tretyakov and S. L. Sokolov, *Tire Design Theory Based on Optimization of Stress-Strain Cycles of its Elements (CSSOT)*, Tire Science and Technology, Vol. 17, No. 2, 1989, pp. 100-108.

[44] Koichu Yamagishi, Minora Togashi, Shinichi Furuya, Kazumi Tsukahara, and Nobuya Yoshimura, *A Study on the Contour of the Radial Tire: Rolling Contour Optimization Theory-RCOT*, Tire Science and Technology, Vol. 15, No. 1, 1987, pp. 3-29.

[45] H. Ogawa, S. Furuya, H. Koseki, H. Iida, K. Sato, and K. Yamagishi, *A Study on the Contour of the Truck and Bus Radial Tire*, Tire Science and Technology, Vol. 18, No. 4, 1990, pp. 236-261.

[46] Y. H. Han, H. S. Choi, S. C. Kang, J. Hwang, and D. Y. Lee, *A Prediction of In-Mold Layout Using a Finite Element Method*, Hankook Tire, 1993.

[47] De Eskinazi, J., Ishihara. K., Volk, H., and Warholic, T. C., *Towards Predicting Relative Belt Edge Endurance With the Finite Element Method*, Tire Science and Technology, Vol. 18, No. 4, 1990, pp. 216-235.

[48] K. Ishihara, *Prediction of tyre belt edge durability using finite element analysis*, Polymer Science and Technology, Vol. 19, No. 9, 1992.

[49] M. Weiss, S. Tsujimoto, and H. Yoshinaga, *Belt Construction Optimization for Tire Weight Reduction Using the Finite Element Method*, Tire Science and Technology, Vol. 21, No. 2, 1993, pp. 120-134.

[50] T. Nemeth, F. Nandori, L. Sarkozi, and T. Szabo, *Application of a Technical Documentation System for Developing New Belt Constructions for Truck Tires*, Tire Science and Technology, Vol. 23, No. 4, 1995, pp. 266-282.

[51] L. O. Faria, J. M. Bass, J. T. Oden, and E. B. Becker, *A Three-Dimensional Rolling Contact Model for a Reinforced Rubber Tire*, Tire Science and Technology, Vol. 17, No. 3, 1989, pp. 217-233.

[52] R. A. Ridha, M. Theves, *Advanced in Tire Mechanics*, Goodyear Techanical Center, Akron, Ohio, USA.

[53] P. Helnwein, C. H. Liu, G. Meschke and H. A. Mang, *A new 3-D finite element model for cord-reinforced rubber composites-Application to analysis of automobile tires*, Finite Element in Analysis and Design, Vol. 14, 1993, pp. 1-16.

[54] G. Meschke, P. Helnwein, *Large-strain 3D-analysis of fibre-reinforced composites using rebar elements: hyperelastic formulations for cords*, Computational Mechanics, Vol. 13, 1994, pp. 241-254.

[55] W. Sprenger, W. Wagner, *On the formulation of geometrically nonlinear 3D-Rebar-elements using the enhanced assumed strain method*, Engineering Structures, Vol. 21, 1999, pp. 209-218.

[56] ABAQUS Theory Manual, Version 5.8.

[57] Melvin F. Kanninen and Carl H. Popelar, Advanced Fracture Mechanics.

Vita

Young-Hoon Han was born in Kyung-Ju, Korea, on December 3, 1960, the son of Jin-Yeon Han and Soo-Hee Sohn. After completing his work at Kyung-Ju High school, Korea in 1978, he entered the Inha University in Korea. He received the degree of Bachelor of Aeronautics in 1983. He was awarded from the Inha University the degree of Master of Science with a major in Mechanical Engineering in 1986. During the following years he was employed as a tire engineer at the Hankook Tire Company. In September 1996 he entered the Graduate School of the University of Texas at Austin. In 1986, he married Ki-Soon Shin. Their children, Jung-Hyun Han, Hyun-Soo Han and Hyun-Jae Han, were born in 1987, 1990 and 1997.

Permanent address: 107-1102 Kumho Town Chungchun-dong Bupyung-ku
Inchon, Korea

This dissertation was typed by the author.